Journal of Innate Immunity

Research Article

J Innate Immun 2022;14:593–614
DOI: 10.1159/000524186

Received: December 21, 2021
Accepted: February 12, 2022
Published online: May 5, 2022

Innate Immune Responses to RSV Infection Facilitated by OGG1, an Enzyme Repairing Oxidatively Modified DNA Base Lesions

Xu Zheng[a] Ke Wang[a] Lang Pan[a] Wenjing Hao[a] Yaoyao Xue[a] Attila Bacsi[a] Spiros A. Vlahopoulos[a] Zsolt Radak[a] Tapas K. Hazra[b] Allan R. Brasier[c] Lloyd Tanner[d] Xueqing Ba[a] Istvan Boldogh[a]

[a]Department of Microbiology and Immunology, University of Texas Medical Branch at Galveston, Galveston, TX, USA; [b]Department of Internal Medicine, University of Texas Medical Branch at Galveston, Galveston, TX, USA; [c]Institute for Clinical and Translational Research, University of Wisconsin-Madison School of Medicine and Public Health, Madison, WI, USA; [d]Department of Clinical Sciences Lund, Respiratory Medicine & Allergology, Lund University and Skåne University Hospital, Lund, Sweden

Keywords
Innate immune response · Respiratory syncytial virus infection · Oxidative DNA base damage · OGG1

Abstract
The primary cause of morbidity and mortality from infection with respiratory syncytial virus (RSV) is the excessive innate immune response(s) (IIR) in which reactive oxygen species (ROS) play key role(s). However, the mechanisms for these processes are not fully understood. We hypothesized that expressions of IIR genes are controlled by the ROS-generated epigenetic-like mark 7,8-dihydro-8-oxo(d)guanine (8-oxo(d)Gua) and 8-oxoguanine DNA glycosylase1 (OGG1). Here, we report that ROS not only generates intrahelical 8-oxo(d)Gua, but also enzymatically disables OGG1 in RSV-infected human airway epithelial cells and mouse lungs. OGG1 bound to 8-oxo(d)Gua in gene regulatory sequences promotes expression of IIR genes, and consequently exacerbates lung inflammation, histological changes, and body weight loss of experimental animals. Pharmacological inhibition of OGG1 substrate binding decreased expression of RSV-induced chemokine and cytokines and significantly lessened clinical symptoms. Results of mechanistic studies show that OGG1 binding at 8-oxo(d)Gua promoter regions modulated loading of transcription factors via transient cooperative interactions in RSV-infected lungs and airway epithelial cells. Other base specific DNA repair proteins had no effects. Collectively, this study identifies unprecedented roles of ROS-generated DNA base lesion(s) and cognate repair protein as a determinant of RSV-induced exuberant inflammation. Pharmaceutical inhibition of OGG1 interaction with its DNA substrate may represent a novel strategy in prevention/intervention of respiratory viral infections.

Introduction

Respiratory syncytial virus (RSV) remains a significant human pathogen worldwide, with over 64 million cases of primary infections recorded yearly [1, 2]. In immunologically naïve or immunocompromised patients RSV spreads from the upper to the lower airways, resulting in life-threatening lower respiratory tract illnesses bronchi-

Karger@karger.com
www.karger.com/jin

Correspondence to:
Istvan Boldogh, sboldogh@utmb.edu

olitis and pneumonia [3, 4]. Presently, there is no safe and effective treatment or RSV vaccine available for prevention and the current management of severe cases is supportive care, similar to severe influenza or SARS-CoV-2 infections [5]. RSV-induced lower respiratory tract illnesses are thought to be driven by excessive and dysregulated innate immune responses (IIRs) that are triggered via signaling pathways generated by host pattern recognition receptors including toll-like receptors, cytoplasmic NOD-like receptors, retinoic acid-inducible gene-I-like receptors, and transmembrane C-type lectin receptors [3, 6–9]. In addition, RSV infection/replication was shown to be a potent inducer of reactive oxygen species (ROS) that significantly contributed to excessive lung inflammation, with the administration of antioxidants significantly decreasing chemokine and cytokine expression and lung pathology [3, 10–12].

ROS are toxic but also act as signaling entities, directly and/or via oxidative modifications to lipids, proteins, and DNA. While oxidatively damaged molecules are generally subjected to degradation, DNA needs to be repaired to maintain genome integrity [13]. Among ROS-induced DNA lesions (oxidized purine, pyrimidine bases, apurinic/apyrimidinic [AP] sites, DNA single- and double-strand breaks), the most abundant is 7,8-dihydro-8-oxo(d)guanine (8-oxo(d)Gua) [14, 15]. It is pre-mutagenic and removed via DNA base excision pathways by base-specific DNA repair enzymes, primarily by 8-oxoguanine DNA glycosylase1 (OGG1) and also by human homolog of *E. coli* Nei-like glycosylases from DNA [13, 16, 17]. The generated AP sites are tailored by AP endonuclease1 to form polymerase-ready 3′OH residues [18]. The generated DNA strand gaps are filled via the short and/or the long-patch repair sub-pathways [13]. ROS also oxidize nucleoside triphosphates (8-oxo-dGTP, 8-oxo-dATP, and 2-OH-dATP) in the cytoplasm, which are removed to prevent their incorporation into DNA by purine nucleoside triphosphates, primarily by the human homolog of *E. coli* MutT 1 [19].

Contribution of ROS to disease severity is supported by multiple observations, while the mechanism is unclear. Because ROS-induced DNA base modifications and DNA repair proteins are linked to gene expression, we hypothesized that their role(s) may link IIRs to RSV infection. To test this hypothesis, immunologically naïve mice and human small airway epithelial cells (hSAEC) were RSV infected and tissue/cell extracts studied using various molecular biological approaches (including chromatin immunoprecipitation coupled quantitative (q) PCR, qRT-PCR, ELISA, Electrophoretic Mobility Shift Assay (EMSA), Western blotting, immunohistochemistry). Results showed that RSV infection increased levels of ROS, intrahelical 8-oxo(d)Gua primarily in transcription start site adjacent promoter sequences along with enrichment of enzymatically disabled OGG1. These interaction(s) in promoters led to expression of cytokines and chemokines, exuberant lung inflammation, histological changes, and body weight loss of experimental animals. Pharmacological inhibition of OGG1, significantly decreased IIRs and inflammation, lessened clinical symptoms and bodyweight loss. Other base lesion specific glycosylases (e.g., NIEL1) and oxidized purine nucleoside triphosphatase, MTH1 had no effect on RSV-induced IIRs. Collectively, these data provide the first evidence for key roles of oxidative DNA base lesion and DNA BER protein(s) controlling dysregulated inflammatory host responses to RSV infection. Importantly, small molecules that prevent OGG1 interaction with 8-oxo(d)Gua are expected to have clinical utility against RSV-induced exuberant lung inflammation.

Methods and Materials

Cell Culture and Reagents

A549 (ATCC, CCL-185) and MLE-12 (ATCC CRL-2110) cells were grown at 37°C and 5% CO_2 in DMEM-F-12 (1:1, Gibco) containing 10% fetal bovine serum (Gibco, Life Technologies, Inc), 100 units/mL penicillin (Gibco), and 100 μg/mL streptomycin (Gibco). hSAEC and CRISPR/Cas9-edited *OGG1* knockout (KO) cells were cultured in small airway epithelial cell basal medium (Promo Cell C-21270), supplemented with supplement pack (C-39170) containing 0.004 mL/mL bovine pituitary, 10 ng/mL extract epidermal growth factor (recombinant human), 5 μg/mL insulin (recombinant human), 0.5 μg/mL hydrocortisone epinephrine, 0.5 μg/mL tri-iodo-L-thyronine, 6.7 ng/mL transferrin (recombinant human), 10 μg/mL retinoic acid, 0.1 ng/mL bovine serum albumin-fatty acid free (BSA-FAF) 2.5 mg/mL; AP endonuclease1' endonuclease activity inhibitor (Cat# CRT0044876; Sigma-Aldrich); TH5487 (4-(4-bromo-2-oxo-3H-benzimidazol-1-yl)-N-(4-iodophenyl)piperidine-1-carboxamide (Cat # HY-125276, Sigma Aldrich; TH2480 (inactive analog of TH5487) is provided by Dr. T. Helleday, Karolinska Institute, Stockholm, Sweden; O8 (Cat# SML1697; Sigma); deferoxamine (Cat# D9533, Sigma); anti-phospho NFκB/RelA/p65 (phosphoserine276) antibody (Ab) (Cat # ab106129); β-actin (Cat# 4970S, CST); anti-FLAG (Cat #F1804, Sigma-Aldrich); NFκB-RelA/p65 (D14E12) (Cat# 8284S, CST), OGG1 (Item #: ENZ-253, ProSpec); Ab to OGG1 (Novus, Cat# NB100-106), Ab to 8-oxo(d)Gua (Millipore Sigma, Cat# MAB3560).

Animals and Infection

BALB/c mice, free of specific pathogens were obtained from The Jackson Laboratories (Bar Harbor, ME USA). Sixteen week-old mice (50% male and 50% female) were used for this study. Mice

Table 1. qRT-PCR primers used in this study

Gene name	Sequence
GAPDH	F: 5′-ACA TCG CTC AGA CAC CAT G-3′ R: 5′-TGT AGT TGA GGT CAA TGA AGG G-3′
TNF	F: 5′-TGC ACT TTG GAG TGA TCG G-3′ R: 5′-TCA GCT TGA GGG TTT GCT AC-3′
IL6	F: 5′-GCA GAT GAG TAC AAA AGT CCT GA-3′ R: 5′-TTC TGT GCC TGC AGC TTC-3′
CXCL10	F: 5′-GAC ATA TTC TGA GCC TAC AGC A-3′ R: 5′-CAG TTC TAG AGA GAG GTA CTC CT-3′
CCL20	F: 5′-CCA TGT GCT GTA CCA AGA GT-3′ R: 5′-TTA GGA TGA AGA ATA CGG TCT GTG-3′
CCL5	F: 5′-TCCTCATTGCTACTGCCCTC-3′ R: 5′-TCGGGTGACAAAGACGACTG-3′
OGG1	F: 5′-CAT ATG AGG AGG CCC ACA AG-3′ R: 5′-CAG AAG ATA AGA GGA CGC AGA AG-3′
NEIL1	F: 5′- GAC AGA GGC AAG TGG CAA AGC A-3′ R: 5′- GCC TCA TTC ACA AAC TGG CTG G-3′
NEIL2	F: 5′- CAT CGA GGA CAA GCC TTA GAA GC-3′ R: 5′- CAC TCA GGA CTG AAC CGA GAG A-3′
OGG1 exon1	F: 5′-GTT AAA CAG CAC CGT GTG GG-3′ R: 5′-TAG AGT ACG ATG CCC CAT GC-3′
OGG1 exon2	F: 5′- TAC CGA GGA GAC AAG AGC CA-3′ R: 5′- GAA GTG GGA GTC CAC GGA AC-3′
OGG1 exon3	F: 5′- CAA GAC CCC ATC GAA TGC CT-3′ R: 5′- GGA TGA GCC GAG GTC CAA AA-3′
OGG1 exon4	F: 5′- GGA GGC TCA TCT CAG GAA GC-3′ R: 5′- CTC CAG GCA GGA TGC AGA G-3′
OGG1 exon5-6	F: 5′- CCT GAT GGC CCT AGA CAA GC-3′ R: 5′- CAT AAG GTC CCC ACA GGC TC-3′
OGG1 exon7	F: 5′- AAG CGC AGA AAG GGT TCC AA-3′ R: 5′- GCC TGG CCT TTG AGG TAG TC-3′
OGG1-F319A	F: 5′- GCC CAA GCG GTG CTG GCC AGT GCC GAC CTG CG-3′ R: 5′- CGC AGG TCG GCA CTG GCC AGC ACC GCT TGG GC-3′
OGG1-H270A	F: 5′- GTG CCC GTG GAT GTC GCT ATG TGG CAC ATT GC-3′ R: 5′- GCA ATG TGC CAC ATA GCG ACA TCC ACG GGC AC-3′
Gapdh	F: 5′- AAT GGT GAA GGT CGG TGT G-3′ R: 5′- GTG GAG TCA TAC TGG AAC ATG TAG-3′
Tnf	F: 5′- AGA CCC TCA CAC TCA GAT CA-3′ R: 5′- TCT TTG AGA TCC ATG CCG TTG-3′
Cxcl2	F: 5′- CAG AAG TCA TAG CCA CTC TCA AG-3′ R: 5′- CTT TCC AGG TCA GTT AGC CTT-3′
Il6	F: 5′-AGC CAG AGT CCT TCA GAG A-3′ R: 5′-TCC TTA GCC ACT CCT TCT GT-3′
Cxcl10	F: 5′-ATT TTC TGC CTC ATC CTG CT-3′ R: 5′-TGA TTT CAA GCT TCC CTA TGG C-3′
Ccl20	F: 5′-CCA GCA CTG AGT ACA TCA ACT-3′ R: 5′-GTA TGT ACG AGA GGC AAC AGT C-3′
Ccl5	F: 5′-ACT CCC TGC TGC TTT GCC TAC-3′ R: 5′-GGC GGT TCC TTC GAG TGA CAA-3′

F, forward primer; R, reverse primer; Gapdh, glyceraldehyde-3-phosphate dehydrogenase.

under mild anesthesia were challenged via the intranasal route with purified RSV (10^6 PFU in 40 μL PBS per mouse), as described previously [10]. Control mice obtained the same volume of PBS. OGG1 inhibitor TH5487 (30 mg per kg) in vehicle (5% glycerol, 5% TWEEN 80 in PBS) was administered via intraperitoneal (i.p.) route [20]. Animal experiments were performed according to the NIH Guide for Care and Use of Experimental Animals and approved by the University of Texas Medical Branch (UTMB) Animal Care and Use Committee (Protocol Number: 0807044D).

RSV Propagation, Purification, Infection, and Titration

The human RSV A2 strain (ATCC VR-1544) was propagated using HEp-2 cells (ATCC CCL-23), cell supernatants collected, virus particles were collected and then purified on discontinuous sucrose gradients (Infant Bronchiolitis and Viral Core. Director Dr Garofalo, Professor, UTMB) as described previously [21]. Aliquots of sucrose purified (cytokine and lipopolysaccharide free) RSV virion (pRSV) suspensions were stored at −80°C until used. For experiments, cell monolayers (80–90% confluence) were infected with pRSV at pre-calculated multiplicity of infection (MOI). After 1 h adsorption, cell monolayers were washed, and culture medium containing 2% FBS was added.

Gene Expression Profiling

At various times after RSV challenge animals were euthanized, lungs excised, and lower airways were homogenized. Total RNAs were isolated using the RNeasy Mini Kit (Qiagen) according to protocols provided by the manufacturer. RNA concentrations were determined on an Epoch Take-3™ system (BioTek, Winooski, VT, USA) using Gen5 v2.01 software. One microgram RNA was reverse transcribed to cDNA using the iScript reverse transcription supermix (Bio-Rad). Equal volumes of individual cDNA preparations (n = 5) were mixed and subjected to the RT^2 Profiler PCR Array (PAMM-011ZD, Mouse Inflammatory Cytokines & Receptors). qRT-PCR was performed using CFX96™ a Real-Time PCR Detection System (Bio-Rad, Hercules, CA, USA). Normalization and data analysis were performed according to the manufacturer's instructions using the web-based software package (https://www.qiagen.com/us/shop/genes-and-pathways/data-analysis-center-overview-page/). The normalization used the average of the following housekeeping genes: beta-D-glucuronidase, beta-2 microglobulin, heat shock protein 90 Alpha (cytosolic) family class A member 1 (Hsp90ab1), glyceraldehyde-3-phosphate dehydrogenase, and cytoplasmic actin 1 (Actb).

Quantitative Real-Time PCR

RSV- and mock-infected cells were lysed and total RNAs were extracted using RNeasy Mini kit (Qiagen) according to the manufacturer's instructions. Crude RNAs were DNaseI-treated and loaded onto RNeasy column and subjected to washes with RW1 and RPE buffers. RNAs eluted with the RNase-free water, included in the kit. The RNA concentration was determined (Epoch Take-3™; BioTek, Winooski, VT, USA) using Gen5 v2.01 software. RNA quality was confirmed by the 260/280 nm ratio (varied between 1.9 and 2.0). 1,000 ng total RNA was used to generate cDNA using the iScript reverse transcription supermix (Bio-Rad). qPCR was performed using specific primers. As internal control cellular GAPDH was used (sequences of primers are listed in Table 1). Changes in mRNA levels were calculated using the $2^{-\Delta\Delta Ct}$ method [22]. Publicly available GEO records can be found at NCBI GSE157630.

CRISPR/Cas9 Genome Editing

OGG1 deletion from hSAECs was performed using Clustered Regulatory Interspaced Short Palindrome Repeat (CRISPR)-associated system (Cas) 9 genome editing as we previous described [20]. In brief, targeting sequences of OGG1 5′-GATGCGGGC-GATGTTGTT GTTGG-3′ and 5′-AACAACATCGCCCGCAT-CACTGG-3′ were cloned into the pSpCas9 (BB)-2A-Puro expression vector. Following vector transfection by Lipofectamine 2000 (Item #: 11668027, ThermoFisher Sci/Invitrogen) into hSAEC, 3 μg/mL of puromycin (Corning, Item #: 61-385-RA) was added and the cells were sub-cultured into 24-well plates and clones were established. Clones were further examined for OGG1 expression by qRT-PCR and Western immunoblotting. OGG1 KO cultures were maintained in SAEC growth medium (PromoCell, Item #: C-21270), containing growth medium supplement mix (PromoCell, item #: C-39175) in the presence of 2 μg/mL puromycin (Corning, Item #: 61-385-RA).

Transfections and siRNA Ablation of Gene Expression

Targeting and non-targeting siRNA was introduced into cell monolayers by using Dharma FECT™ Transfection Reagents per the manufacturer's instructions (Dharmacon; Horizon, Perkin Elmer). Expression vectors introduced into semi-confluent monolayers by using Lipofectamine 2000 (Invitrogen). In brief, transfected cells were incubated in recommended transfection media at 37°C for 4 h, followed by replacement with complete media. Transfection efficiency or levels of gene silencing was evaluated with RT PCR and Western blotting. The RT-PCR primer are shown in Table 1.

Construction of OGG1 Variants and Sequencing

The cDNAs encoding wild type (WT) FLAG-hOGG1, FLAG-K249Q, and FLAG-F319A mutants were cloned into the eukaryotic expression vector pcDNA3.1(+) as we documented previously [23]. Sequence fidelity of inserts for WT OGG1 and variants (K249Q and F319A) were determined using Applied Biosystems 3130XL Genetic Analyzer, followed by post-detection processing in The Molecular Genomics Core of UTMB (Director, Steven Widen, PhD) https://www.utmb.edu/mgf/molecular-genomics-core/sequencing.

Assessment of Cytokine/Chemokine Levels

Broncho-alveolar lavage fluid (BALF) was analyzed for secreted cytokines/chemokines using multiplex immunoassays. In brief, BALF samples were clarified by centrifugation (800 *g* for 5 min at 4°C) and the levels of cytokines quantitated using the Bio-Plex Pro™ Mouse Cytokine Assay (Cat #: 12009159, Bio-Rad, Hercules, CA, USA). Recombinant cytokine samples were used as standards. Readings were performed on a Bioplex® 200™ system (Bio-Rad). Data were analyzed using Bio-Plex Manager™ Software Version 6.0 Build 617 (Bio-Rad).

Evaluation of Airway Inflammation and Clinical Scores

Responses of airways to RSV infections were examined as described previously [10–12]. After euthanasia, tracheae were cannulated, and lungs were lavaged by two instillations of 0.6 mL of ice-cold PBS. BAL fluid samples were centrifuged (800 *g* for 5 min at 4°C), and the resulting supernatants were stored at −80°C for further analysis. Total cell counts in the BALF were determined from an aliquot of the cell suspension using a hemocytometer and

Table 2. qPCR primers used in this study for chromatin precipitation assays

Gene name	Sequence
TNF (–350 to –120 bp)	F: 5′-GGT CCC CAA AAG AAA TGG AGG-3′ R: 5′-TTT ATA TGT CCC TGG GGC GA-3′
IL6 (–267 to –117)	F:5-GCA GAT GAG TAC AAA AGT CCT GA-3′ R: 5′-TTC TGT GCC TGC AGC TTC-3′
CXCL10 (–179 to 71 bp)	F: 5′-AGG GAA ATT CCG TAA CTT GGA GGC-3′ R: 5′-TTC ATG GTG CTG AGA CTG GAG GTT-3′
CCL20 (–366 to –170 bp)	F: 5′-TGT TCC TGT GTG GGG CTG-3′ R: 5′-TTG CCA CAT GGG GTT TTC C-3′
CCL5 (–156 to 29 bp)	F: 5′-AGA CTC GAA TTT CCG GAG GC-3′ R: 5′-TCC ACG TGC TGT CTT GAT CC-3′
Tnf (–252 to –55 bp)	F: 5′-GCC CCA GAT TGC CAC AGA AT-3′ R: 5′-GCT CTC ATT CAA CCC TCG GA-3′
Il6 (–106 to 65 bp)	F: 5′-CCC CAC CCT CCA ACA AAG ATT-3′ R: 5′-CAG AGA GGA ACT TCA TAG CGG T-3′
Cxcl10 (–134 to 8 bp)	F: 5′-AGC AAT GCC CTC GGT TTA CA-3′ R: 5′-CCG GCT GCT GAG GAG TAT TT-3′
Ccl20 (–116 to –44 bp)	F: 5′-TTG TGG TGA CAG GAT GAG GC-3′ R: 5′-GAG TTG ATG TAC TCA GTG CTG G-3′
Ccl5 (–93 to 100 bp)	F: 5′-TGT GGA AAC TCC CCA AGT CC-3′ R: 5′-CAG AGA TCT TCA TGG TAC CCG C-3′

then cytospin preparations were made using a Shandon CytospinR 4 Cytocentrifuge (Thermo Scientific, Waltham, MA, USA). Cells were stained with Modified Wright-Giemsa using HEMA-TEK 2000 Slide Stainer (Protocol) for differential cell counts. Differential cell counts were performed on cytocentrifuge preparations in a blind fashion by two independent researchers counting 1,000 cells from each animal.

Lungs were removed and fixed in 10% buffered formalin, followed by paraffin embedding. Four-μm cross-sections were stained with hematoxylin and eosin. The slides were analyzed and scored for cellular inflammation by a certified pathologist with expertise in mouse lung, unaware of the length of infection and sections identities. On tissue sections, the extent of lung inflammation, perivasculitis, bronchiolitis, alveolitis were examined. Minimum ten fields for each section were examined and analyzed to determine whether observed differences were statistically significant among groups. Randomly selected fields were photographed using an OLYMPUS Microscope System BX53P microscope with a built-in digital CCD color camera DP73WDR.

Clinical illness grading scale for mice was established previously [10]. Individual mice were scored as follows 0 = healthy; 1 = barely ruffled fur; 2 = ruffled fur but active; 3 = ruffled fur and inactive; 4 = ruffled fur, inactive, and hunched; 5 = dead. In addition, body weight loss was determined daily and used to monitor the progression of disease over the experimental period.

Assessment of Lung' and Cellular Redox State

Mice were challenged with pRSV (10^6 PFU per lung) and lungs were collected at 1, 2, 4, 6, 12, and 24 h post infection (hpi). Levels of oxidatively modified proteins in RSV-infected lungs were determined by using Protein Carbonyl Assay Kit according to the manufacturer's recommendations and as described previously [24, 25]. Lung tissue lysates were derivatized with 4-dinitrophenylhydrazine (DNPH) for 15 min followed by incubation at room temperature with a neutralization buffer. Equal amount of protein lysates were fractionated using SDS-PAGE. Proteins were blotted on Pure Nitrocellulose membranes (BIO-RAD 162-0112) and membranes were blocked overnight and incubated with anti-DNP Ab (ab178020; 1:5,000) in 5% nonfat dry milk overnight at 4°C. Levels of oxidized proteins were visualized by chemiluminescence using the ECL kit (Amersham™).

Intracellular ROS levels were determined by using the fluorogenic probe 5- (and-6)-chloromethyl-2′7′-dichlorodihydrofluorescein diacetate acetyl ester (CM-H_2DCFDA; Invitrogen, Eugene, OR) [26, 27]. In brief, hSAEC cells were mock- or RSV-infected and loaded with 10 μM CM-H2DCF-DA at 37°C for 10 min, various times after RSV infection. Cells were then washed with PBS and lysed (50 mM Tris-HCl, pH 7.5, 150 mM NaCl, 1 mM EDTA, 1 mM EGTA, 1% NP-40), then clarified by centrifugation. Changes in DCF fluorescence in supernatant fluids were determined by using a Synergy H1 Hybrid Multi-Mode Reader (BioTek) with excitation/emission at 485 nm/535 nm. Results are expressed as changes in fluorescence units (FU).

Amplex® UltraRed (10-acetyl-3,7-dihydroxyphenoxazine; Invitrogen, Eugene, OR, USA) assays were carried out as we previously described [26]. Briefly, hSAECs were RSV-infected (MOI = 1) and aliquots of serum free culture media were mixed with reaction buffer containing 50 μM Amplex® UltraRed and 0.05 U/mL

Table 3. Probes used for electro mobility shift assays*

Probe	Sequence
Probe containing 8-oxo(d)Gua and NFκB binding motif (derived from Cxcl2 promoter)	Sense: 5′-TTCCCTGGTCCCCGGGCTTTTCCAGACATCG-3′ Anti-sense:5′-biotin-CGATGTCTGGAAAAGCCCGGGGACCA**G***GGAA-3′
Probe containing NFκB binding motif	Sense: 5′-TTCCCTGGTCCCCGGGCTTTTCCAGACATCG-3′ Anti-sense: 5′-biotin-CGATGTCTGGAAAAGCCCGGGGACCAGGGAA-3′
Cold probe containing 8-oxo(d)Gua and NFκB binding motif	Sense: 5′-TTCCCTGGTCCCCGGGCTTTTCCAGACATCG-3′ Anti-sense: 5′-CGATGTCTGGAAAAGCCCGGGGACCA**G***GGAA-3′

G* signifies 8-oxo(d)Gua. The NFκB binding motif is underlined.

of horse reddish peroxidase (optimal concentrations were determined in preliminary studies). Changes in resorufin fluorescence were determined at 560 nm and 620 nm (excitation and emission, respectively) by using a BioTek FLx800 fluorimeter. To establish the standard curve, increasing concentrations of H_2O_2 (0–10 μM) was used. The addition of catalase (5 U/mL, Sigma-Aldrich, St. Louis, MO, USA) decreased H_2O_2 levels by ~98%.

Chromatin Immunoprecipitation Assay

Cells expressing FLAG-OGG1, anti-FLAG (F1804; Sigma-Aldrich) were used. Chromatin immunoprecipitation assay (ChIP) assays were performed as described previously [28–30]. Briefly, 10^7 cells expressing FLAG-tagged-OGG1 for each sample (or lung tissues, 20 mg wet weight) were cross-linked in 1% formaldehyde at 37°C for 5 min. For lung tissues, 50 mg (wet weight) were cross-linked. After washing with chilled PBS, the cells were re-suspended (lungs homogenized) in 300 μL of lysis buffer. The DNA was sheared by sonication and chromatin was incubated with specific antibodies (anti-FLAG Ab or OGG1 Ab (Novus)) or isotype control IgG for 2 h and collected using Protein A/G Magnetic beads (MAGNA0017; Millipore). Magnetic beads were washed and the immunoprecipitated DNA was eluted in elution buffer (1% SDS and a $NaHCO_3$) at 65°C for 2 h. Of note, all buffers used during these procedures contained the antioxidant deferoxamine mesylate to prevent further DNA oxidation [31]. The precipitated DNA was phenol/chloroform-extracted, precipitated with 100% ethanol, and abundance of ChIP-ed DNA was determined by qPCR. The ChIP primers are shown in Table 2.

Electrophoretic Mobility Shift Assay

Nuclear extracts (NEs) were prepared using CelLytic™ Nuclear™ Extraction Kit (Cat # NXTRACT, Sigma) and protein concentrations were quantified by Pierce BCA Protein Assay Kit (Cat # 23225, Thermo Scientific). EMSA assays were performed as described previously [29, 32]. Briefly, biotin-labeled probes (Table 3; 20 fmol) were mixed with NE (2 μg) in buffer containing 10 mM Tris-Cl (pH 8.0), 10 mM NaCl, 1 mM DTT, 1 mM EDTA, 1 mg/mL BSA, and 0.1 μg/μL Poly[d(I-C)]. In controls, recombinant p50 (2.75 ng) and p65 (3.75 ng) were annealed in 10 mM Tris (pH 7.5), 5 mM NaCl, 1 mM DTT, 1 mM EDTA by incubation at 37°C for 60 min. Protein-DNA complexes were resolved on a 6% DNA retardation gel (Invitrogen, Item # EC6365BOX) in 0.25 × TBE buffer (100 V for 2 h) and visualized by using Amersham Imager 680 (Global Life Sci. Sol. Marlborough, MA, USA). Band intensities were quantified using Image J v1.51 (U. S. NIH, Bethesda, MD, USA).

Oligonucleotide Excision Assay

OGG1 glycosylase activity on 8-oxo(d)Gua containing DNA was assessed as we described previously [33, 34]. Sequences of 5′-end Cy5-labeled probes and location of 8-oxo(d)Gua are shown in Table 2. In brief, 100 fmol of the Cy5-labeled probe (/5′-Cy5/-AGAGAAGAAGAAGAAGA A/8oxodG/AGATGGGTTATTC-GAACTAGC-3′) were incubated with increasing concentrations (0.5, 1, or 2 pmol of OGG1 (Item #: ENZ-253, ProSpec)) in 10 μL digestion buffer (10 mM of Tris-HCl [pH 7.5], 10 mM of NaCl, 1 mM of EDTA, 1 mg/mL BSA, and 1 mM of DTT). After incubation for 10 min at room temperature, the reaction was halted by adding 10 μL loading buffer (containing 8 μL of formamide, 10 mM of NaOH) and heated for 5 min at 95°C. The cleaved product was separated from the intact probe in a 15% polyacrylamide gel containing 8 M urea in Tris-borate-EDTA buffer (pH 8.4). The separated bands were visualized by using Amersham™ Imager 680.

Immunoblotting

Cells were lysed using cell lysis buffer (Cell Signaling Technology; Item #: 9803; 50 mM Tris-HCl, pH 7.5, 150 mM NaCl, 1 mM EDTA, 1 mM EGTA, 1% Nonidet P-40) containing 2.5 mM sodium pyrophosphate, 1 mM glycerophosphate and protease inhibitors (1 mM Na_3PO_4, 1 mM NaF, and 20 μg/mL aprotinin, leupeptin, phenylmethanesulfonyl fluoride). Equal amounts of proteins were separated by SDS-PAGE electrophoresis and transferred into nitrocellulose membranes, blocked with 5% nonfat dry milk in TBS-T (20 mM Tris base, 500 mM NaCl, and 0.05% Tween-20, pH 7.5) and then incubated for 3 h with primary Ab and subsequently with horseradish peroxidase-conjugated secondary Ab (1:4,000 dilution; Southern Biotech, Birmingham, AL, USA). The signals were detected using the ECL Plus chemiluminescent detection system (Bio-Rad, Item #: 1705061). Equal loading was confirmed using the β-Actin Ab (Cat # 4970S; Cell Signaling Technology).

Assessment of Oxidatively Modified OGG1

Cells expressing FLAG-OGG1 were RSV infected (MOI = 1) for 0, 3, 6, 12, 18, and 24 h and nuclei were isolated and lysed in a de-oxygenized buffer containing 50 mM Tris-HCl (pH 7.5), 50 mM NaCl, 1 mM EDTA, 1 mM EGTA, 1% Nonidet P-40, 2.5 mM sodi-

um pyrophosphate, protease inhibitor mixture (Sigma), 100 μM diethylenetriaminepentaacetic acid, 5 mM iodoacetamide, 200 units/mL catalase, and cysteine sulfenic acid probe, DCP-Bio1 (0.1 mM 3-(2,4-dioxocyclohexyl) propyl (DCP)) conjugated to biotin (Millipore Sigma) [29, 35]. Nuclear extracts were clarified, and the supernatants were incubated with 30 μL of protein G-Sepharose (Millipore Sigma) at 4°C for 1 h, precleared and incubated with Ab against FLAG for 3 h and added to protein G-Sepharose for 3 h. The immune-precipitates were resolved by SDS-PAGE, and OGG1 oxidized at cysteine was detected by streptavidin-conjugated horseradish peroxidase-coupled chemiluminescence.

Fluorescent Microscopy

hSAECs were plated on collagen pretreated cover glasses (Roche Applied Sciences) were transfected, mock- or RSV-infected. Cells were fixed with acetone-methanol (1:1) for 20 min and permeabilized using 0.1% (wt/vol) Triton X-100 diluted in phosphate-buffered saline (PBST) for 5 min. Cells were blocked by IgG (10 μg per mL) in presence of 1% BSA for 1 h at room temperature and primary antibodies were added as at a dilution recommended by the manufacturer or determined in preliminary studies (1–100; 1–300) in PBST for 1 h at 37°C. Ab to OGG1 (Novus, NB100-106), anti phospho-RelA Ab (Novus, Nb100-2176). After washing cells in PBST (3 times), secondary Ab conjugated to Alexa Fluor 488 (goat anti-rabbit) or Alexa Fluor 594 (goat anti-mouse) was added for 1 h at 37°C. Cells were dried and mounted with Vecta shield/DAPI, 4′6-diamidino-2-phenylindole hydrochloride (Vector Laboratories, Burlingame, CA, USA). Over 30 randomly selected fields of view per sample were photographed using a WHN10×/22 eyepiece and a ×60 objective (field of view is 1.1 mm and camera correction is 0.63) on an OLYMPUS Microscope System BX53P.

Cell Viability Assay

Cells were treated with increasing concentrations (0, 2.5, 5, 10, 20 μM) of TH5487 or solvent every 8 h. Cell culture medium was harvested at 48 h to perform the colorimetric lactate dehydrogenase assay (LDH; Abcam, Item # ab102526). The assay was performed using a 96-well plate according to manufacturer instructions. The output of triplicate samples was determined immediately (T1), 10 min (T2), 20 min (T3), 30 min (T4) at OD 450 nm on a microplate reader (Synergy H1 Hybrid Multi-Mode Reader; BioTek) at 37°C protected from light. The amount of LDH in the media was calculated using ΔA450 nm = (A2 – A1) formula, where: A1 is the sample reading at time T1. A2 is the sample reading at time T2. LDH activity was expressed in nmol of NADH generated by LDH during the reaction time (ΔT = T2 – T1). LDH activity = (BI (ΔTx V)) × D = nmol/min/mL, B = amount of NADH in sample, calculated from standard curve (nmol). ΔT = Reaction time (minutes). V = Original sample volume added into the reaction well (mL). D = Sample dilution factor.

Statistical Analysis

Statistical analyses were performed using Microsoft Office Excel Student's *t* test to analyze differences between the means of two groups. The data are expressed as the mean ± SEM. Differences were considered significant at $p < 0.05$ (*$p < 0.05$, **$p < 0.01$, ***$p < 0.001$, ****$p < 0.0001$).

Results

Inhibition of OGG1 DNA Substrate Binding Decreases RSV-Induced Lung Inflammation

Unlike clinical infections, where RSV spreads from the upper to lower airways, we delivered purified infectious virions (10^6 PFU/lung) to the lungs of naïve mice to induce IIRs and disease as described previously [10–12]. Parallel groups of infected mice were mock- (vehicle/solvent) or treated with a small molecule inhibitor (TH5487) of OGG1 (i.p. 30 mg/kg, a dose selected based on results published previously) [20]. Mice were euthanized (0 h, 12 h, 24 h), BAL fluid and lungs were collected to determine gene expression at RNA and protein levels and asses histological changes. Overall changes of RNA levels were determined using qRT-PCR profiler arrays. After subtracting changes resulting from mock-challenge of lungs expression levels of 36 chemokines, cytokines and receptors were modulated out of 86 included in the array. Out of 36, 23 C-C and C-X-C motif-containing proinflammatory mediators were significantly increased by 12 h (online suppl. Fig. 1, Table 1; for all online suppl. material, see www.karger.com/doi/10.1159/000524186). At 24 hpi only *Ccl8* (MCP2) showed a significant increase (>50-fold) in addition to those expressed at 12 hpi (online suppl. Fig. 1b). Compared to RSV-infected mock-treated control, pharmacologically-induced OGG1 deficiency significantly decreased (50–80%) expression of 16 genes (*Ccl2, Ccl20, Ccl7, Csf2, Csf3, Cxcl1, Cxcl13, Cxcl5, Cxcl9, Il1a, Il1b Osm, Tnf, Tnfsf11*) and receptors (*Il10ra, Il1rn*). Interestingly, expression from ten genes were increased >3-fold (*Ccl1, Ccr8, Ifny, Il13, Il17a, Il17b, Il21, Il3, Il5r, Tnfs4*) in the presence of OGG1 inhibitor.

In children with severe RSV bronchiolitis TNF, CC20, IL6, CCL5, and CXCL10 were reported to be the primary inflammatory markers along with excessive neutrophilia in BAL fluid and nasopharyngeal washings [36–38]. Therefore, changes at mRNA levels of these mediators were further validated by individual qRT-PCR for each mouse (Fig. 1a). Our data indicate that inhibition of OGG1 by TH5487 (that prevents OGG1 from engaging its DNA substrate [20]) significantly decreased RNA levels of *Tnf*, *Ccl20*, *Il6*, *Ccl5*, and *Cxcl10* (Fig. 1a) as well as protein levels (TNFα, CCL20, IL6, CCL5, and CXCL10) in lungs and BAL fluid, respectively (Fig. 1a). Changes in protein levels for additional soluble inflammatory mediators (CXCL13, CXCL5, CCL11, CCL12, CCL3, CCL17, CCL19, CCL2, CCl22, CCL24, CCL4, CCL7, CXCL1, CXCL11, CXCL12, CXCL16, IL1b, IL10, IL16, CSF, MCP3) are summarized in online supplementary Figure 2.

As expected from expression of inflammatory mediators there were excessive number of neutrophils (1.85×10^5 per mL at 12 hpi and 2.2×10^5 at 24 h) in BAL fluid of infected/untreated animals (Fig. 1c, d). Administration of the OGG1 inhibitor to infected animals significantly decreased the number of neutrophils (Fig. 1c, d). Histological analyses of lungs showed excessive accumulations of inflammatory cells primarily around bronchioles and as-

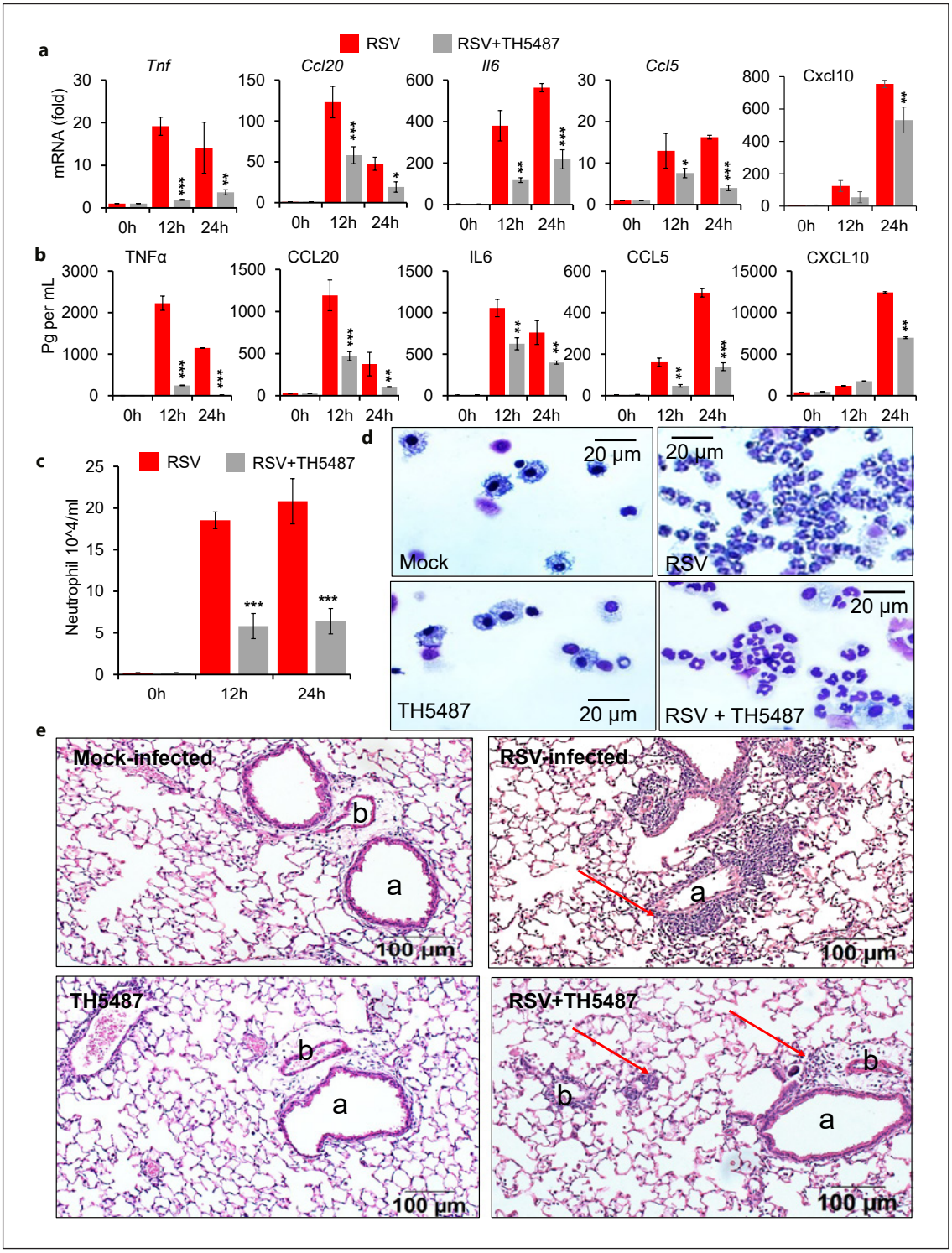

1

(Figure continued on next page.)

sociated blood vessels, with pharmacologically induced OGG1 deficiency decreasing neutrophil influx (Fig. 1e). These results imply that non-ciliated small epithelial cells were the primary site of chemokine/cytokine expressions in response to RSV infection as documented previously [39]. Because our goal was to examine the role of OGG1 in RSV-induced innate gene expression, lung histological changes were not further investigated. However, we assessed biological consequences of host IIRs and RSV replication by determining weight loss and clinical signs of illness as described previously [10–12]. These results show that inhibition of OGG1 by TH5487 provides a large degree of protection against RSV-induced weight loss and improves clinical scores (Fig. 1f, g) compared to those animals receiving solvent. Together, these data imply that OGG1 not only played significant role(s) in RSV infection-induced IIRs but also in manifestation of its biological consequences.

Ablation of OGG1 Decreased Expression of IIR Genes in RSV-Infected hSAECs

Parallel cultures of OGG1 KO hSAECs ($hSAEC^{OGG1-}$, generated by CRISPR/Cas9 genome editing, Fig. 2a–c) and OGG1 proficient hSAEC (puromycin resistant $hSAEC^{OGG1+}$) were RSV infected and inflammatory gene expressions were determined. Appropriate MOI, time points and toxicity of TH5487 were determined in preliminary studies (online suppl. Fig. 3a–h). Data show that RSV infection (MOI = 1) of $hSAEC^{OGG1+}$ increased expression of *TNF*, *CCL20*, *IL6*, *CCL5*, and *CXCL10* by 75-, 28-, 125-, 18- and 52-folds, respectively (Fig. 2d). In contrast, in $hSAEC^{OGG1-}$ RSV-induced expressions were limited to an average of 19.5-, *7-*, *33-*, *8.5-*, *and 11-fold for TNF*, *CCL20*, *IL6*, *CCL5*, and *CXCL10*, respectively (Fig. 2d). To exclude the possibility that antibiotic (puromycin) selection was related to decreased gene expression, OGG1 was depleted by small interfering RNA (siR-

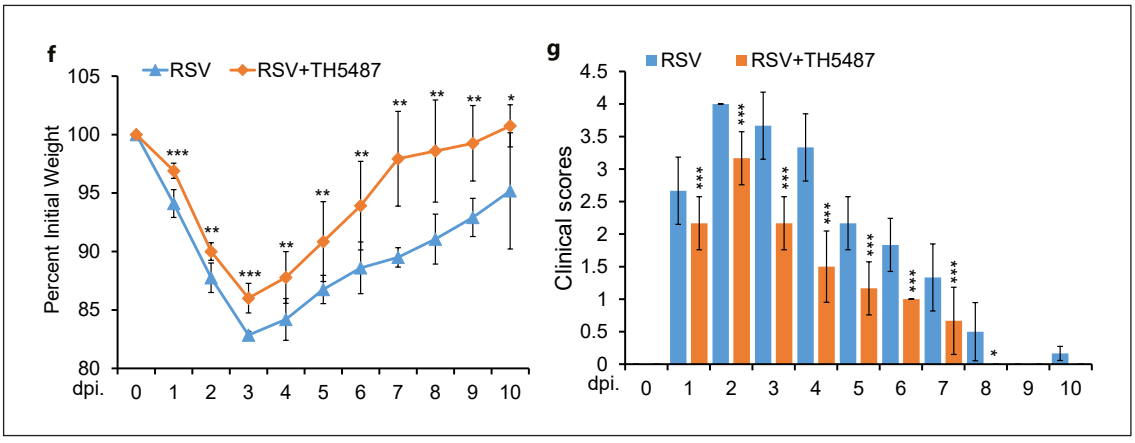

Fig. 1. OGG1 inhibition decreases RSV-induced expression of inflammatory mediators and morbidity. **a**, **b** Inhibition of OGG1 DNA substrate binding by TH5487 decreases expression of proinflammatory mediators in RSV-infected lungs. **a** Changes in RNA levels of *Tnf*, *Ccl20*, *Il6*, *Cxcl10*, and *Ccl5*. **b** Protein levels of TNF, CCL20, IL6, CCL5, and CXCL10 in BAL fluid ± TH5487. Each data points represent $n = 5$. Changes in levels of additional inflammatory mediators are shown in online suppl. Fig. 2. **c** Numbers of neutrophils in BAL fluid after RSV infection without and with TH5487. BAL fluids were derived at 0, 12, 24 hpi and cells on cytospin slides stained with Modified Wright-Giemsa. For each point over 1,000 cells were counted ($n = 5$). **d** Representative images showing abundance of neutrophils before and 24 h after RSV infection in BAL fluid of mock- and TH5487-treated mice. Images were photographed using an OLYMPUS Microscope System (BX53P) with a built-in digital CCD color camera DP73WDR. Magnification: 40x lens and 3.6x (camera). Scale bar, 20 µm. **e** Representative images of H&E-stained lung sections from mock- and RSV-infected animals with and without inhibition of OGG1. Panels: upper left, lung of mock-infected, solvent-treated mice; upper right, inflammatory infiltrates surrounding perivascular, peribronchial regions and alveoli in lungs of RSV-infected mice (solvent-treated); lower left, lung section of TH5487-treated mice; lower right, lung section of RSV-infected, TH5487-treated mice. Scale bar, 100 µm. Bronchus, bronchi (**a**); Blood vessel (**b**). Images were photographed using an OLYMPUS microscope as in legend to **d**. **f**, **g** Pharmacological inhibition of OGG1 decreases morbidity of infected animals. Parallel groups of RSV-infected mice treated i.p with TH5487 or solvent. Weight of mice recorded daily, and loss depicted as the percent of initial weight (**a**). Clinical scores determined as in Materials and Methods. $n = 9$). dpi, days post infection. Student's *t* test were utilized analyze differences between groups. In (**a**, **b**) *Tnf*, TNFα, tumor necrosis factor alpha; *Ccl5*, CCL5, chemokine (C-C Motif) ligand 5 (RANTES); *Ccl20*, CCL20, chemokine (C-C motif) ligand 20 (or MIP-3-Alpha); *Cxcl10*, CXCL10, C-X-C motif chemokine ligand 10 (interferon-inducible cytokine IP-10); *Il6*, IL6, interleukin-6 (interferon, beta 2). Lower case and capital letters are symbols of gene/mRNAs and proteins, respectively. In (**a–c**) data are mean ± SEM $^*p < 0.05$, $^{**}p < 0.01$, $^{***}p < 0.001$.

NA) (Fig. 2e, lower panel) and were RSV-infected (as above). In controls, hSAECs were transfected with non-targeting siRNA. Compared to the non-targeting siRNA-transfected cells, OGG1-depleted hSAECs expressed significantly lower levels of *TNF* (57- vs. 18-fold) *CCL20* (48- vs. 19-fold), *IL6* (34- vs. 12.5-fold), *CCL5* (14- vs. 8.1-fold), and *CXCL10* (143- vs. 49.5-fold) (Fig. 2e). In controls, depletion by siRNA of endonuclease VIII-like 1 (NEIL1) (excises 8-oxo(d)Gua, 2,6-diamino-4-hydroxy-5-formamidopyrimidine (FapyGua) from DNA [40] or MTH1 [19]) had no significant effect on gene expression (Fig. 2f). Similar results were obtained after siRNA depletion of

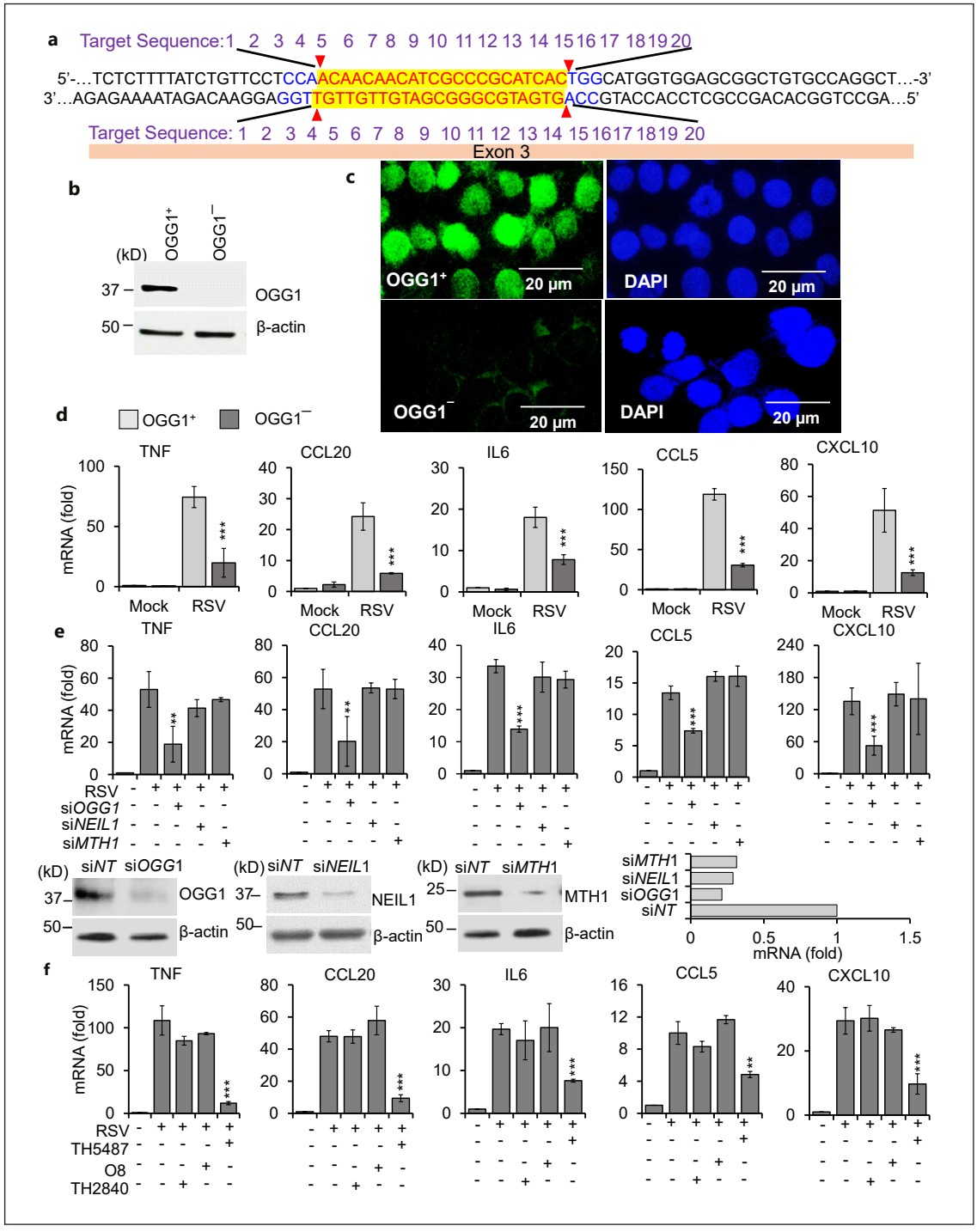

2

(For legend see next page.)

OGG1, NEIL1, or MTH1 in A549 cells (online suppl. Fig. 3i). Taken together, these results imply that OGG1, but not other oxidatively modified guanine base-processing enzymes affected gene expression in RSV-infected cells.

To further validate the role of OGG1 in inflammatory gene expression, hSAECs were treated with TH5487 (10 μM, an effective nontoxic dose; online suppl. Fig. 3f, g) 1 h before (−1 h) and +2 h after RSV adsorption, at 10 and 18 hpi (its half-life is ~6 h in cell cultures) [20]. Changes in RNA levels were determined at 24 hpi. Compared to mock-treated RSV infected hSAECs, expressions decreased from 121- to 18-fold, 49- to 8.5-fold, 21- to 8-fold, 11.5- to 5-fold and from 31- to 9.5-fold for *TNF*, *CCL20*, *IL6*, *CCL5*, and *CXCL10,* respectively (Fig. 2f). Inhibitory effect of the TH5487 on RSV-induced inflammatory gene expression was similar in A459 cells (online suppl. Fig. 3h). The inactive analog of TH5487, TH2480 [20], or O8 (inhibits glycosylase activity but not OGG1 substrate binding [41]) showed no effects (Fig. 2f; online suppl. Fig 3h). Taken together, these results show that inhibition of OGG1 substrate binding decreased proinflammatory gene expression in human airway epithelial cells.

RSV Infection Enriched OGG1 on Promoters of Proinflammatory Genes

Mock- and RSV-infected lungs were harvested at 12 hpi (time of excessive expression of chemokines and cytokines), chromatin-protein complexes were crosslinked, processed and IP-ed by using OGG1 Ab. RSV infection resulted in an average of 14-, 16-, 11-, 7.5-, and 19-fold increases in enrichment of OGG1 on regulatory sequences of *Tnf, Ccl20, Il6, Ccl5, and Cxcl10*, respectively (Fig. 3a). Importantly, TH5487 decreased OGG1 enrichment by 84%, 85%, 75%, 61%, 82% for *Tnf, Ccl20, Il6, Ccl5, and Cxcl10*, respectively (Fig. 3a). Mock challenge of lungs, or TH5487 or vehicle (administered i.p.) did not result in OGG1 enrichment.

OGG1 was reported to scan DNA for its substrates (8-oxo(d)Gua and Fapy(d)Gua) via migrating along DNA strands [42]. This process raised the possibility that protein-DNA crosslinking captured OGG1 bound to Fapy(d)Gua (or nonspecifically). Therefore, OGG1 Ab-ChIP-ed DNAs were IP-ed using Ab to 8-oxo(d)Gua (does not bind to FapyGua [31, 43] and subjected to qPCR. Results show that compared to IgG control, there was increased 8-oxo(d)Gua levels in OGG1 Ab ChIP-ed DNA of lungs (average *34-, 14-, 10-, 7-, and* 19-fold for *Tnf*, *Ccl20, Il6, Ccl5, and Cxcl10*, respectively) (Fig. 3b). In controls, there were no detectable changes in oxidatively modified cytosine as shown by ChIP assays (online suppl. Fig. 4a).

To demonstrate that OGG1 enrichment also occurs in human cells, FLAG-tagged OGG1 expressing hSAECs were RSV-infected (MOI = 1). Results show that RSV-infection induced an average of 12-, 15-, 8-, 6- and 9-fold increases in OGG1 enrichment within *TNF*, *CCL20*, *IL-6*, *CCL5* and *CXCl10* promoter sequences, respectively (Fig. 3c). TH5487 (10 μM) decreased, while its inactive analog TH2840 had no effect on levels of ChIP-ed DNA (Fig. 3c). Another OGG1 inhibitor O8 [41] substantially increased levels of ChIP-ed promoter sequences using Ab to FLAG (Fig. 3c). To test for 8-oxo(d)Gua in FLAG Ab-ChIP-ed DNAs they were IP-ed using 8-oxo(d)Gua-Ab (as above). Compared to IgG control, Ab to 8-oxo(d)Gua enriched levels of IP-ed sequences an average of 19-, 25-, 31-, 17- and 16-fold within *TNF*, *CCL20*, *IL-6*, *CCL5,* and *CXCl10* promoter, respectively (Fig. 3d). Oxidative modifications to guanines are in line with RSV infection-induced increase in protein carbonyl levels in lungs (online suppl. Fig. 4b) and ROS levels in hSAECs (online sppl. Fig. 4c, d).

Fig. 2. OGG1 knockdown, siRNA depletion or inhibition of OGG1 substrate binding decreased RSV-induced proinflammatory gene expressions. **a** Schematic depiction of OGG1 knockdown by CRISP/Cas9 technology. Lack of OGG1 expression as shown by Western blotting (**b**) and microscopic imaging (**c**). Nuclei of cells were counter stained with DAPI. Images were photographed using an OLYMPUS Microscope System as in Fig. 1d. Magnification, 20x lens and 3.6x (camera). Scale bar, 20 μm. **d** OGG1 KO (OGG1^{-}) hSAECs expressed significantly lower levels of *TNF, CCL20, IL6, CCL5,* and *CXCL10* in response to RSV infection. **e** SiRNA depletion of *OGG1* but not *NEIL1* or *MTH1* decreased proinflammatory gene expression (*TNF, CCL20, IL6, CCL5,* and *CXCL10*) in hSAECs. Lower panels, extent of OGG1, NEIL1, and MTH1 silencing as determined by Western blotting and qRT-PCR. siNT, nontargeting siRNA. **f** Inhibition of OGG1 substrate binding by TH5487 decreased inflammatory gene expression. The O8, inactive analog of TH5487, TH2480 had no effect. In (**b–d**), Cells were RSV-infected (MOI = 1) and total RNAs were isolated at 24 h. Data are mean ± SEM. ***$p < 0.001$; **$p < 0.01$. NEIL1, human ortholog of *E. coli* Nei; *MTH1,* hMTH1; TH5487, 4-(4 bromo-2-oxo 3H-benzimidazol-1-yl)-N-(4-iodophenyl)piperidine-1-carboxamide; O8 (3,4-dichloro-benzo[b]thiophene-2-carboxylic acid hydrazide). In (**b**–**d**); *TNF, CCL20, IL6, CCL5,* and *CXCL10* as in legend to Fig. 1. hMTH1, human homolog of *E. Coli* MutT 1. DAPI, 4,6-diamidino-2-phenylindole.

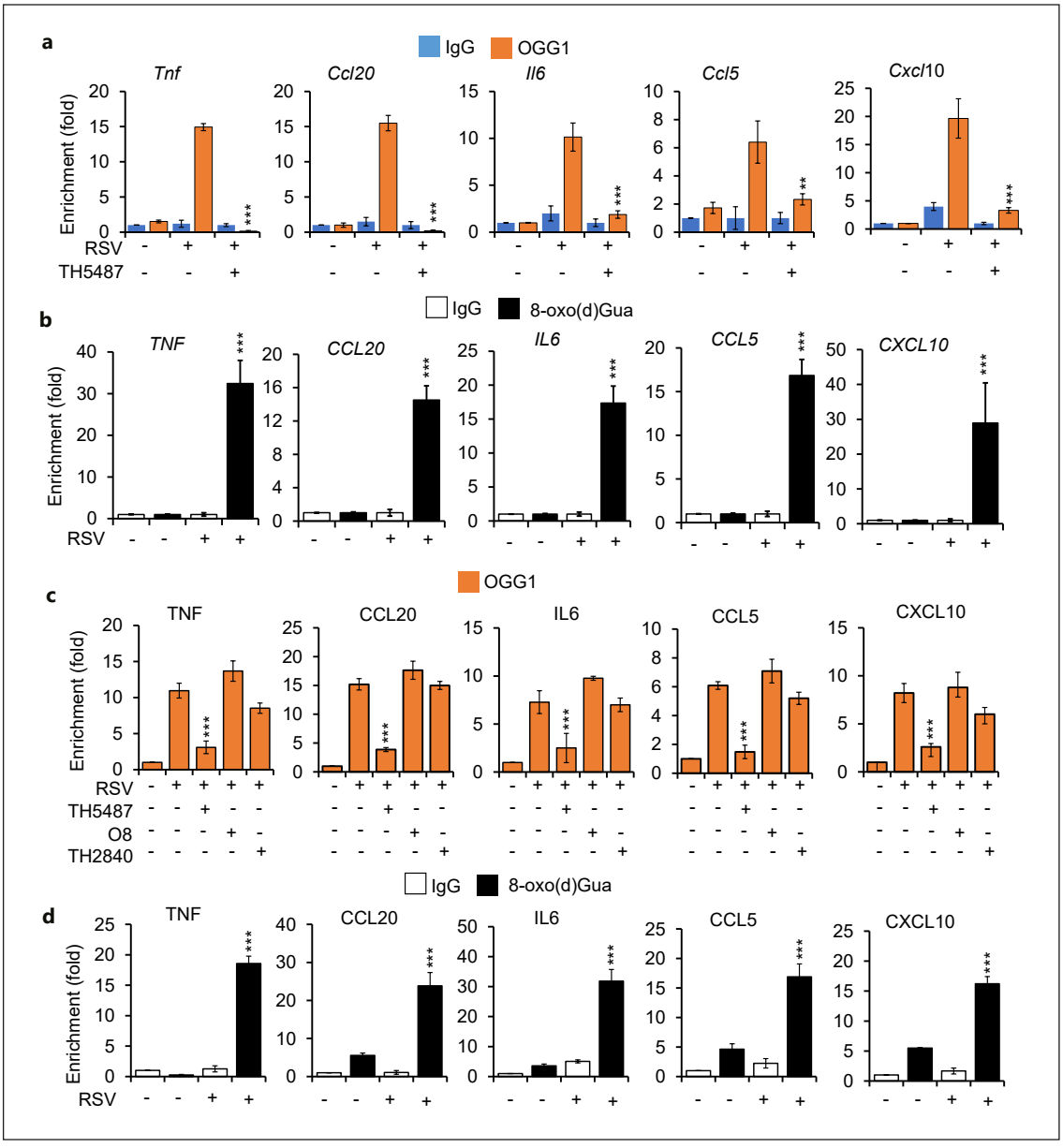

Fig. 3. RSV infection induced OGG1 enrichment on TSS proximal promoter regions. **a** Enrichment of OGG1 in TSS-adjacent promoter sequences of *Tnf*, *Ccl20*, *Il-6, Ccl5, and Cxcl10* was inhibited by TH5487. Mouse lungs were mock- or RSV-challenged and ±TH5487 treated. Cross-linked DNA-protein-complexes were isolated and ChIP assays were performed by using Ab to OGG1 (n = 5). **b** OGG1-ChIP-ed TSS-adjacent sequences contained the OGG1 substrate, 8-oxo(d)Gua. OGG1-Ab ChIP-ed DNAs were isolated and then IP-ed by using 8-oxo(d)Gua specific Ab or IgG. **c** RSV infection induced OGG1 enrichment on TSS-adjacent sequences of inflammatory genes in hSAECs. FLAG-OGG1-expressing hSAEC cultures were infected with RSV (MOI = 1), and solvent- or TH5487-, TH2480-, or O8-treated. DNA-protein complexes were ChIP-ed using Ab to FLAG(OGG1). ChIP-ed DNAs were analyzed by qPCR. **d** Presence of 8-oxo(d)Gua in OGG1(FLAG Ab)-ChIP-ed DNA. ChIP-ed DNAs were isolated and then IP-ed by using 8-oxo(d)Gua specific Ab or IgG and levels of sequences in IPs were determined by qPCR. In (**a–d**), ***$p < 0.001$; **$p < 0.01$. In (**a–d**): *TNF, CCL20, IL6, CCL5,* and *CXCL10* as in legend to Fig. 1. TSS, transcription start site.

J Innate Immun 2022;14:593–614
DOI: 10.1159/000524186

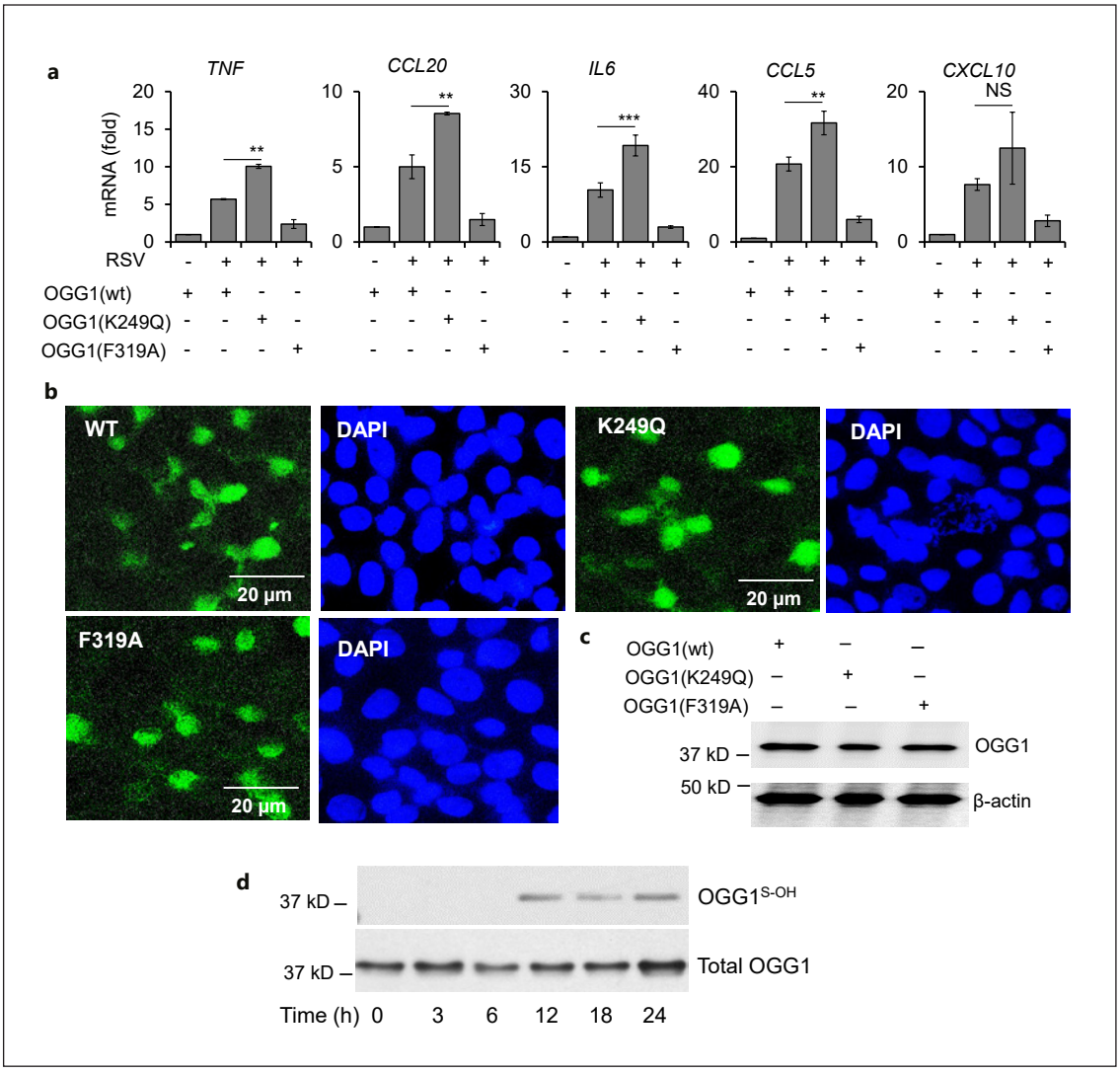

Fig. 4. Enzymatic activities of OGG1 is dispensable for RSV-induced inflammatory gene expression. **a** OGG1 defective in base excision activities promotes gene expression. FLAG-tagged WT and mutant OGG1s (K249Q and F319A) were transgenically expressed in parallel hSAEC^{OGG1-} cultures and mock- or infected with RSV (MOI = 1). Cells harvested at 24 hpi and total RNAs were isolated to determine expressions of *TNF*, *CCL20*, *IL6*, *CCL5*, and *CXCL10* by qRT-PCR. Data are mean ± SEM. ***$p < 0.001$; **$p < 0.01$. In a, *TNF, CCL20, IL6, CCL5,* and *CXCL10* as in legend to Fig. 1. **b**, **c** Expression levels of FLAG-tagged wtOGG1, K249Q, F319A in hSAEC^{OGG1-}. Parallel cultures of hSAEC^{OGG1-} were processed for fluorescence microscopy (**b**) or immunoblotting (**c**) at time of RSV infection (legend to **a**) using Ab to FLAG. Nuclei were stained with DAPI. Images were photographed using an OLYMPUS Microscope System as in legend to Fig. 1d. Magnification, ×20 lens and ×3.6 (camera). Scale bar, 20 μm. **d** Oxidative modification to OGG1 on cysteine residues after RSV infection. Parallel cultures of cells expressing FLAG-OGG1 were RSV-infected (MOI = 1) for 0, 3, 6, 12, 18, and 24 h and nuclei were isolated to detect oxidized OGG1 (OGG1^{S-OH}) by using cysteine sulfenic acid probe DCP-Bio1 as in Materials and Methods. DAPI, 4,6-diamidino-2-phenylindole.

RSV-Induced Inflammatory Gene Expression without Requiring OGG1 Enzymatic Activity

To examine whether OGG1 enzymatic activity was needed for gene expression, we utilized WT and enzymatically defective OGG1 mutants. Parallel cultures of hSAEC^{OGG1-} cells were transfected with vectors expressing FLAG-tagged wtOGG1, the lysine 249 glycine mutant (K249Q), that lacks base excision activity but retained the ability to recognize/bind 8-oxo(d)Gua in DNA [44] or the Phenyl alanine 319 Alanine mutant OGG1 (F319A) that have been shown to have poor affinity for 8-oxo(d)Gua in DNA and thus lack BER activity [45]. FLAG-OGG1

variants-expressing hSAEC^{OGG1-} were mock- or RSV-infected (MOI = 1) and harvested at 24 h. Intriguingly, the K249Q mutant significantly increased expression from *TNF* (from 6- to 11.5-fold), *CCL20* (from 5.2- to 8.9-fold), *IL6* (from 11-fold to 19.6-fold), *CCL5* (from 20.5- to 31.8-fold), and *CXCL10* (from 8.4 to 12.2-fold) compared to WT (Fig. 4a). Expression of the F319A variant in hSAEC-$^{OGG1-}$ displayed reduced facilitation of RSV-induced expression from IIR genes, compared to those hSAEC^{OGG1-} expressing wtOGG1 or the K249Q mutant (Fig. 4a). Expression of WT and mutants OGG1 varied between 45 and 50% and were nearly equal in hSAEC^{OGG1-} as shown by microscopic imaging and Western blotting, respectively (Fig. 4b, c). The enhanced expression of proinflammatory mediators by the enzymatically inactive OGG1 mutant (K249Q) implies that enzymatic activities of OGG1 were dispensable for gene expression. Comprehensive studies have indicated that cysteine residues were essential for OGG1 enzymatic activities and its structural stability [46] and were prone to oxidation [47]. These results suggest that host cells repurposed OGG1 via cysteine oxidation in RSV infected cells. To test this possibility, we utilized DCP-Bio1 reagent [29], and observed OGG1 oxidative post-translation modification at cysteine in nuclei of RSV infected cells (Fig. 4d). Taken together, these data suggest that OGG1 binding to promoter but not its enzymatic activities were required for gene expression in RSV-infected cells.

OGG1 Couples NFκB to Expression of IIR Genes in RSV-Infected Lungs and hSAECs

Reports indicate that RSV infection triggered persistent activation of NFκB, and other transcriptional regulators were causally related to inflammatory gene expressions, consequently the exuberant inflammation [48–50]. Taking the decreases in RSV-induced gene expressions in hSAEC^{OGG1-} or in lungs by the OGG1 inhibitor TH5487, a potential interplay between OGG1 and NFκB was evaluated. OGG1 depleted hSAECs were RSV-infected and levels of RelA/NFκB at promoters of *TNF*, *CCL20*, *IL6*, *CCL5*, and *CXCL*10 were determined. ChIP assays showed significant decreases in promoter-associated RelA/NFκB, compared to those ChIP-ed from cells transfected with control siRNA (Fig. 5a, b). Pharmacological inhibition of OGG1 substrate binding by TH5487 resulted in similar decreases in RelA/NFκB enrichment on gene promoters in RSV-infected hSAECs (Fig. 5b) as well as in A549 and MLE-12 cells (online suppl. Fig. 5a–d). NEIL1 ablation had no effect on RelA/NFκB binding (Fig. 5a). Another OGG1 inhibitor, O8, substantially increased promoter enrichment of RelA/NFκB (Fig. 5b) in line with lack of its capacity to prevent substrate binding [41]. The inactive analog of TH5487, TH2480 [20] had no effect on DNA occupancy of RelA/NFκB in the chromatin (Fig. 5b). To rule out the possibility that decreased proinflammatory gene expression by OGG1 deficiency was due to impaired activation of RelA/NFκB, and its nuclear translocation, data show that RSV infection induced phosphorylation of RelA at serine^{276} and nuclear translocation of pRelA/NFκB were not affected in hSAECs (Fig. 5c, d) and A549 cells (online suppl. Fig. 6). Importantly, inhibition of OGG1 substrate binding by TH5487 significantly decreased RelA/NFκB enrichment on promoters of *Tnf*, *Ccl20*, *Il6*, *Ccl5*, and *Cxcl10* in lungs of infected mice (Fig. 5e).

To ascertain that inhibition of OGG1 substrate binding decreased RelA/NFκB DNA occupancy, DNA-protein complexes were isolated from lungs, ChIP-ed using Ab to OGG1, and then mixed with recombinant RelA/NFκB. Results of re-ChIP experiments showed that Ab to RelA/NFκB efficiently pulled down OGG1 Ab-ChIP-ed DNA (Fig. 6a) and imply that OGG1 bound to its substrate (8-oxo(d)Gua) within the same segment of *Tnf*, *Ccl20*, *Il6*, *Ccl5*, and *Cxcl10* promoter. These results along with those showing that TH5487 decreased RelA/NFκB-driven proinflammatory gene expression and inflammation, strongly suggest that RelA/NFκB binding is interlinked with OGG1, on the promoter of these genes in RSV-infected cells. To further this hypothesis, NEs were isolated from RSV-infected OGG1-expressing hSAECs and NFκB binding to intact and 8-oxo(d)Gua containing DNA probes (Table 2) were examined using EMSA. As shown in Figure 6b, binding of RelA/NFκB was significantly higher to 8-oxo(d)Gua containing DNA compared to that probe with guanine, suggesting that OGG1 in NE promotes RelA/NFκB DNA occupancy. To test if indeed OGG1 in NEs made the difference in RelA/NFκB binding, we utilized TH5487. TH5487 alone had no effect on recombinant (r)NFκB DNA occupancy (Fig. 6c). Inhibition of OGG1 substrate interaction in probe by TH5487, decreased NFκB binding in NE affecting both RelA(p65)-p50 and p50-p50 (hetero and homo-dimmers) in a concentration dependent manner (Fig. 6d, left and right panels). In controls, OGG1 antagonist inhibited OGG1 binding to probes containing 8-oxo(d)Gua (Fig. 6e), while TH2840 and O8 had no effect on OGG1 binding (Fig. 6f). Together, these results suggest that OGG1 at genomic 8-oxo(d)Gua promotes RelA/NFκB DNA occupancy in regulatory sequences of inflammatory genes. Importantly, these results strongly suggest

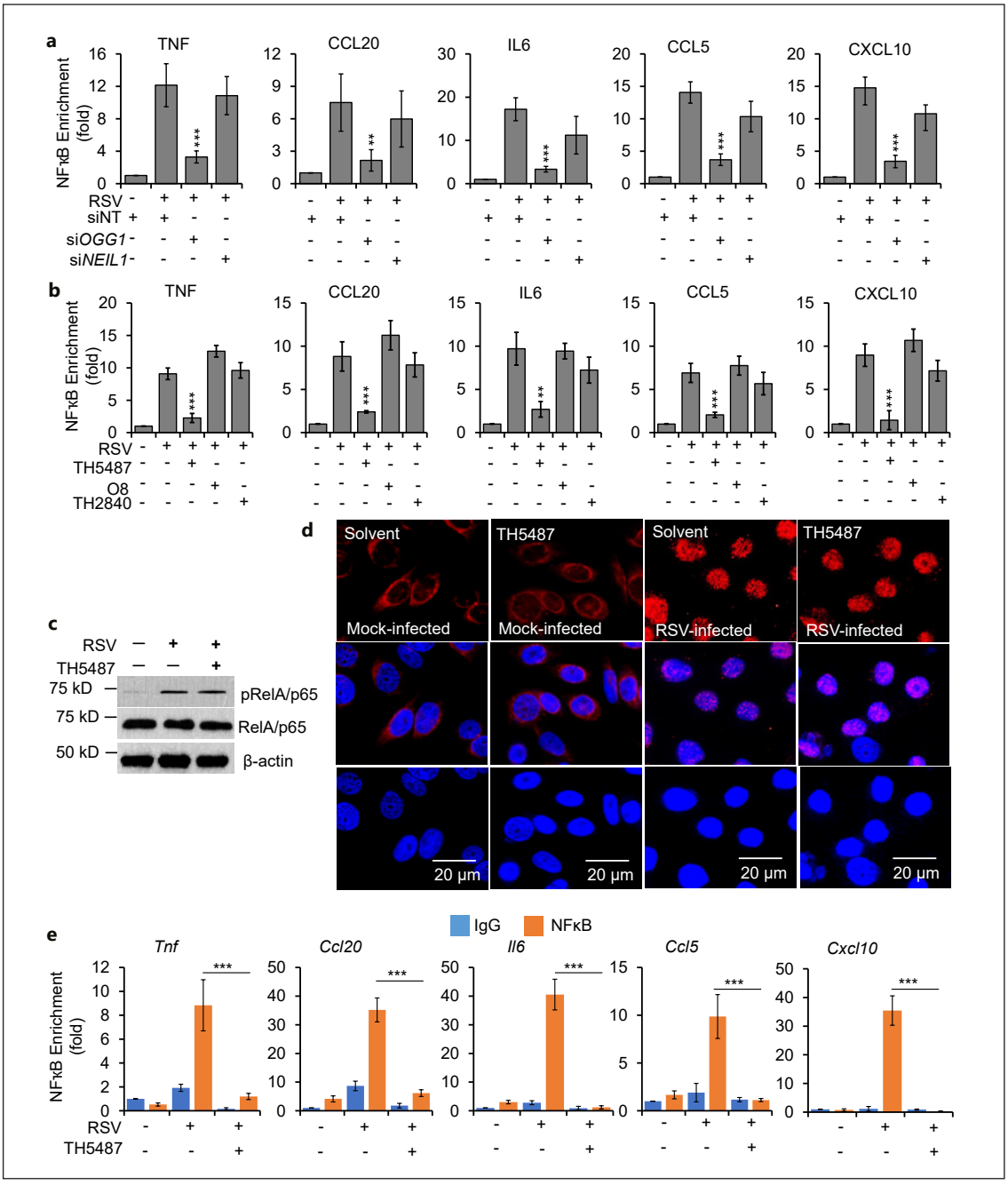

Fig. 5. OGG1 promotes NFκB DNA occupancy in RSV-infected cells. **a** OGG1 but not NEIL1 increases promoter occupancy of NFκB. Parallel cultures of hSAECs were OGG1 and NEIL1 depleted by siRNA and RSV-infected (MOI = 1). Binding of NFκB to promoter sequences of *TNF, CCL20, IL6, CCL5, and CXCL10* was determined by ChIP assays using Ab to RelA/p65. **b** The OGG1 inhibitor decreases enrichment of RelA/NFκB on gene promoters. Parallel hSAECs treated and RSV-infected for 24 h. Levels of RelA/NFκB bound to promoter sequences were determined as in legend to **a**. **c**, **d**, OGG1 inhibitor TH5487 had no effect on phosphorylation and nuclear translocation of RelA/NFκB. hSAECs were RSV-infected (MOI = 1) ±TH5487 (10 μM) for 24 h and changes in phosphorylated RelA/NFκB at ser^{276} in NEs was determined by Western blotting and microscopic imaging. Cell were counter stained with DAPI. Randomly selected fields were photographed using an OLYMPUS Microscope System as in Fig. 1d. Magnification: ×60; scale bar, 40 μm. The experiments were performed twice with two biological replicates each. **e** Inhibition of OGG1 substrate binding decreases in RelA/NFκB' DNA occupancy in lungs. Mice ($n = 5$) challenged with RSV (10^6 PFU per lung) mock- or TH5487-treated and lungs were excised (12 hpi). RelA/NFκB promoter enrichment were determined by ChIP assays. In (**a**, **b**, **e**, **f**), ***$p <$ 0.001; **$p < 0.01$. *TNF*, *CCL5*, *CCL20*, *CXCL10*, *IL6* as in legend to Fig. 1. DAPI, 4,6-diamidino-2-phenylindole.

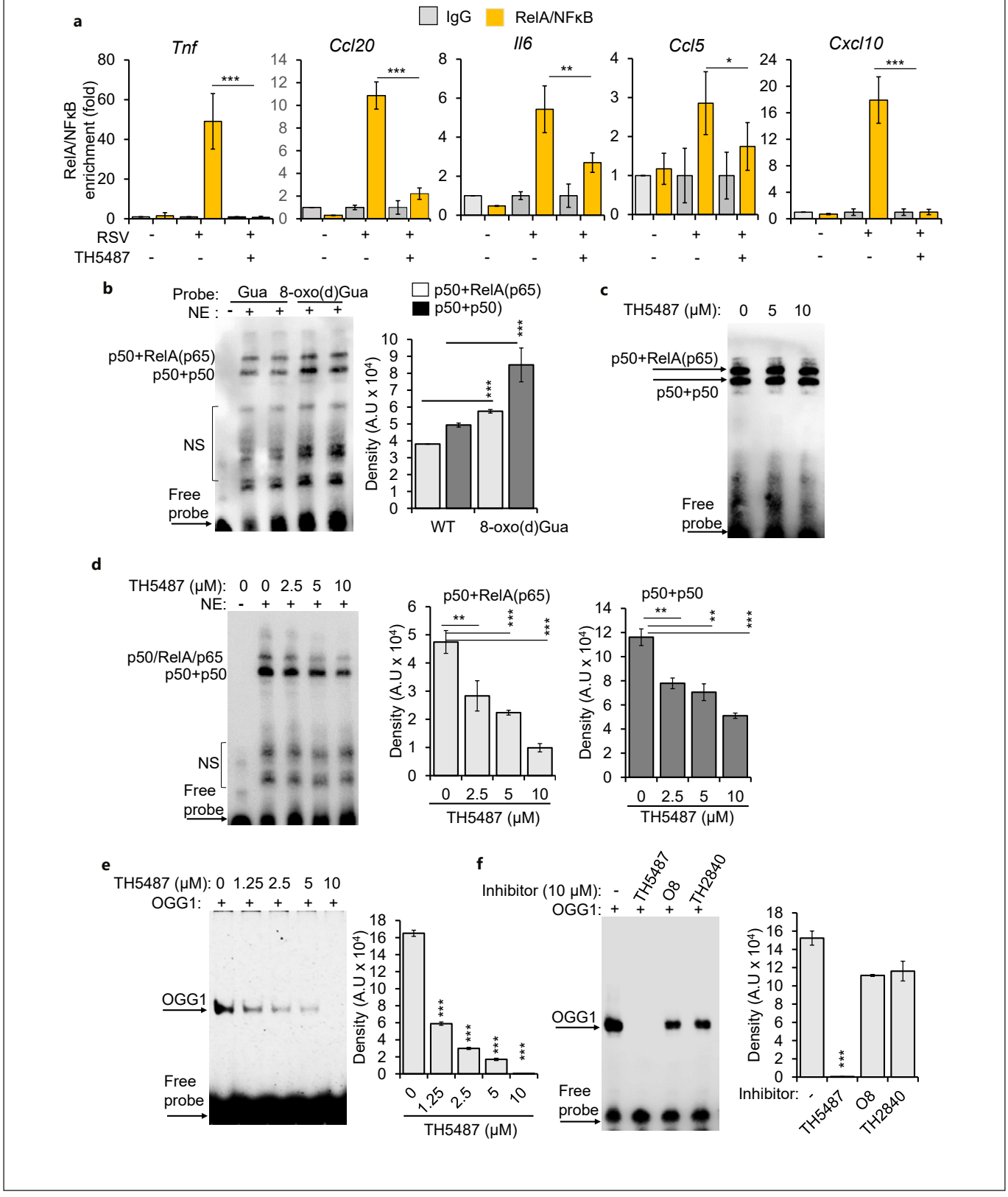

(For legend see next page.)

that TH5487 inhibited inflammatory gene expression via interrupting this mechanism in RSV-infected cells/airways.

Discussion

RSV is one of the most important viral agents causing frequent hospitalizations in young children, immunocompromised adults and elderly. Presently, there is no effective vaccine or treatment available. IIR(s) by the host to RSV infection not only facilitate efficient clearance of the virus but also contribute to the pathogenesis of respiratory diseases. While many molecular details of RSV-induced expression of proinflammatory mediators and inflammation are well defined, the mechanisms by which ROS facilitate IIR processes lack clarity. In this study, we demonstrate that ROS rapidly induce DNA base modifications primarily 8-oxo(d)Gua in guanine-rich promoters and paradoxically inactivated the cognate DNA BER protein OGG1 oxidatively. OGG1 stalled at its substrate, promotes NFκB DNA occupancy, consequently cytokine and chemokine expression, leading to exuberant inflammation and lung pathology. In support of these observations, inhibition by small molecules of OGG1 substrate binding, silencing, or its knockdown significantly decreased RSV-induced IIRs and clinical scores. Other DNA base lesion repair proteins had undetectable roles. Thus, our study has identified a previously unprecedented interplay between ROS-induced DNA base damage, initial steps in DNA BER, DNA occupancy of transcription factors, and IIRs. Pharmaceutical inhibition of OGG1 interaction with its substrate may represent a novel strategy in prevention/intervention of respiratory viral infections.

Intrapulmonary infection with RSV rapidly increased expression of over thirty cytokines and chemokines, at RNA and protein levels, which are associated with the "cytokine storm." This is followed by a rapid influx of neutrophils into airways, and severe symptoms leading to significant body-weight loss in line with observation described previously [7, 39, 51–53]. Although mechanism(s) of RSV-induced cell activation signaling in robust IIRs was not specifically investigated in this study, it may include those signaling pathways generated by interaction of virions with cellular attachment/fusion receptors via viral glycoprotein G, fusion (F) protein, in addition to activation of cell membrane toll-like receptors and intracellular sensors including retinoic acid-inducible gene-I-like receptors, MAVs, NOD-like receptors (Fig. 7) [3, 9, 54–59]. Signaling through these receptors also lead to an imbalance in cellular redox via activation of cytoplasmic and mitochondrial oxidoreductases and decreases in levels of the transcription factor NF-E2-related factor 2 due to its degradation resulting in decreased antioxidant cellular defenses [3, 60, 61]. In our experiments, the timing and magnitude of RSV-induced increase in ROS levels, correlated well with increase in levels of 8-oxo(d)Gua in transcription start site-adjacent promoter regions and with inducible expressions of epithelial innate cytokine and chemokines in lungs and hSAECs. Interestingly, there were no detectable changes in levels of 5-hydroxyuracil a product of oxidized cytosine(s) in these G:C-rich gene regulatory sequences implying not only specificity but sensitivity of guanines to ROS [15, 62]. Of note, cytosine oxidation result in an unstable intermediate (5,6-dihydroxy-5,6-dihydrocytosine), which either dehydrated, deaminated or undergo reactions to form 5,6-dihydroxy-5,6-dihydrouracil, or 5-hydroxyuracil the most frequent oxidation product [14]. While these findings are novel for RSV infection, other reports provide supportive

Fig. 6. OGG1 promotes NFκB DNA occupancy in RSV-infected cells. **a** OGG1 and NFκB bound in close proximity within TSS-adjacent promoter sequences. Mice were RSV-infected and treated as in legend to Fig. 5e. Chromatin were OGG1-Ab ChIP-ed, DNA isolated and recombinant RelA/NFκB was added then re-ChIP-ed by Ab to RelA/p65. Gray column, IgG; orange column, Ab to RelA/NFκB. **b** Increased binding of RelA/NFκB to DNA probes containing 8-oxo(d)Gua. NEs isolated from RSV-infected OGG1 expressing hSAECs were mixed with DNA probes lacking (lanes 1,2) or containing 8-oxo(d)Gua (lanes 3,4) and subjected to EMSA. **c** TH5487 had no effect on (r)RelA/NFκB binding to 8-oxo(d)Gua-containing DNA. Recombinant (r) p50 and p65 proteins were annealed, mixed with 8-oxo(d)Gua-probe and EMSA was performed. **d** OGG1 inhibitor in NE decreased NFκB′ DNA occupancy on 8-oxo(d)Gua containing probe. NEs were isolated from RSV-infected hSAECs and mixed with 8-oxo(d)Gua-containing probe and EMSA performed. Right panels, graphical depiction of band intensities*. **e** Concentration dependent inhibition of OGG1 binding to 8-oxo(d)Gua containing DNA by TH5487. OGG1 was incubated with probes at 4°C for 15 min and complexes were subjected to EMSA. **f** TH5487 but not O8 or TH2480 inhibits OGG1 DNA binding. OGG1 was incubated with inhibitors for 15 min at 4°C ± inhibitors, mixed with 8-oxo(d)Gua-probes then EMSA performed. In (**a**) ***$p < 0.001$; **$p < 0.01$. *Tnf, Ccl5, Ccl20, Cxcl10, Il6* as in legend to Fig. 1. In (**b**, **c**, **d**, **e**, **f**), images were captured by using Amersham™ 680 Imager. ***$p < 0.001$; **$p < 0.01$. *Band intensities were determined by using Image J v.5 (2 experiments with biological replicates).

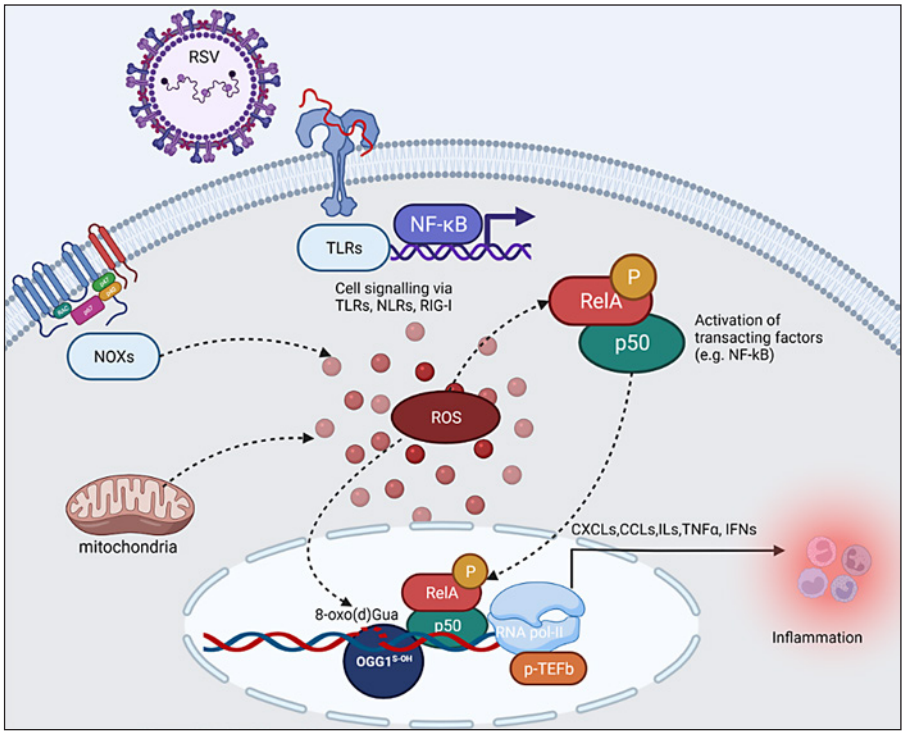

Fig. 7. Inflammatory gene expression in RSV-infected cells is controlled by oxidatively repurposed DNA repair protein OGG1 bound to 8-oxo(d)Gua. In response to RSV infection, parallel overlapping signaling cascades are activated by TLRs, NLRs, RIG-I, and ROS. Signaling through these receptors and ROS activate and induce nuclear translocation of transcription factors, as exemplified here by NFκB. ROS also induce oxidative modification of DNA bases, among which 8-oxo(d)Gua functions as an epigenetic-like mark. The oxidatively disabled OGG1, stalled at 8-oxo(d)Gua, nucleates binding of transcription factors. OGG1$^{S\text{-}OH}$, OGG1 cysteine sulfenic acid; 8-oxo(d)Gua, 8-Oxo-7,8-dihydro-2′-deoxyguanosine; NOX, NADPH oxidases; RelA, viral-rel avian reticuloendotheliosis viral oncogene homolog A, NFκB subunit; p50, nuclear factor kappa-B DNA binding subunit; CXCLs, CCLs, C-X-C and C-C motif containing chemokines; ILs, interleukins, TNF, tumor necrosis factor; IFNs, interferons; TLR, toll-like receptor; NLR, NOD-like receptor; RIG-I, retinoic acid-inducible gene-I-like receptor.

evidence for etiological link between increases in ROS levels, generation of 8-oxo(d)Gua in gene regulatory regions and G-quadruplex(es)-containing DNA sequences after cytokine or LPS exposures of cells, or under hypoxic conditions, respectively [63–65].

RSV-induced expression of IIR genes at mRNA and protein levels were significantly altered when OGG1 binding to genomic substrate was pharmacologically inhibited in lungs. Interestingly, out of the genes altered in response to RSV-infection, the OGG1 inhibitor, TH5487 down-regulated sixteen, while expressions from ten genes were upregulated, implying uncharacterized roles of OGG1 in gene expression. Of note, although quantity and quality of the innate inflammatory mediators expressed in response to RSV infection are determinant of disease severity, viral clearance, adaptive immune responses, and lasting immunity (rev in [9, 66], here we discuss mechanism(s) by which DNA repair protein(s) regulate gene expression.

Under physiological conditions, OGG1 constitutes the frontline defense for the repair of 8-oxo(d)Gua (and Fapy(d)Gua) [13, 14]. In RSV-infected cells, 8-oxo(d)Gua was not removed from regulatory regions of genes investigated here, but OGG1 was enriched on them, as shown by ChIP-coupled qPCR. To further this observation, we found that cysteine residues in the OGG1 polypeptide were oxidized to sulfenic acid by ROS leading to loss of its glycosylase activity. These data are in line with results from previous studies showing that ROS and/or cysteine modifying agents reversibly suspended OGG1 glycosylase activity [47]. Similarly, cytokine- or LPS-induced ROS caused significant decreases in OGG1 repair activity via oxidation of its critical cysteine residues and it enriched in gene regulatory sequences both in cultured cells and lungs [29, 34, 46]. Due to ROS in RSV-infected cells, cysteine oxidation was a very-likely scenario; however, other post-translational modifications can't be excluded. To further support the role of enzymatically inactive OGG1 in gene expression, we show that K249Q OGG1 mutant that capable of scanning DNA, but remains tightly associated with chromatin for extended time periods upon 8-oxo(d)Gua recognition [67] promoted expression of IIRs genes. In contrast, expression of OGG1(F319A) that has low affinity for 8-oxo(d)Gua [45] did not support inflammatory gene expression. Along with our data showing cysteine-sulfenic acid containing OGG1 in RSV-infected cells and importance of cysteine(s) in OGG1' enzymatic activity, we propose that OGG1 modified at cysteine(s) is the primary driver of gene expression in oxidatively stressed cells.

Reports have shown that activation of NFκB by ROS signaling and by RSV infection-triggered signaling from

cellular receptors/sensors was the primary transacting factor, which drove expression of innate inflammatory network (proinflammatory CXC, CC chemokines, and cytokines, type I and III interferons) [68, 69]. Specifically, NFκB bound to its cis-element recruits the positive transcriptional elongation factor-b (a complex of cyclin dependent kinase 9 and bromodomain containing protein 4 [a pleiotropic chromatin remodeling complex that directly mediated transcriptional elongation of mRNAs and increased proinflammatory gene expression in RSV-infected cells [6, 7, 30, 70, 71]. Our results, however, show that pharmacologically induced OGG1 deficiency, or its knockdown significantly decreased expression of inflammatory mediators that are primarily dependent on NFκB in RSV-infected lungs and in hSAECs. Lack of OGG1 had no effect on NFκB activation or nuclear translocation indicating that OGG1 deficiency might have caused altered DNA occupancy of NFκB. Studies by ChIP assays indeed showed that lack of OGG1 lowered the level of NFκB bound to promoters and expression of IIR genes in RSV-infected lungs and hSAECs. These observations are supported by electro mobility shift assays, showing increased NFκB binding to 8-oxo(d)Gua-containing DNA. Previous studies have shown that OGG1 bound to 8-oxo(d)Gua in proximity of the NFκB-binding motif, increased binding of both homodimeric and heterodimeric NFκB over 10-fold compared to that of NFκB alone. The mechanism by which OGG1 increases NFκB binding is subject of speculation; however, we propose that OGG1-induced DNA architectural changes (bending/twisting DNA as part of DNA base excision repair [72]) allow the recognition of binding motif(s) in chromatin and lower the energy needed for NFκB binding [29]. The exact molecular nature of the interaction(s) between OGG1 and NFκB on the chromatin requires additional studies.

Pharmacologically induced OGG1 deficiency significantly lowered both expression from IIR genes, inflammation and clinical disease after RSV infection. Another chemically different small-molecule inhibitor (SU0268) that inhibit OGG1 substrate binding significantly decreased airway inflammation and improved survival of experimental animals after infection with *Pseudomonas aeruginosa* [73]. The common mechanism among various models is that RSV, LPS-, TNFα-, or *Pseudomonas* challenge increase ROS levels in cells/lungs, consequently generate 8-oxo(d)Gua (epigenetic-like mark [64]) in gene promoters as well as enzymatically inactivate OGG1. In support, addition of O8 to RSV-infected cells increased expressions from IIR genes. Although molecular mechanism of this phenomenon should be further investigated, our interpretation was that O8 did not inhibit OGG1 binding, nor interaction with and nor insertion of 8-oxo(d)Gua into the active site pocket or DNA bending, but inhibited glycosylase activity, which supported NFκB binding and consequent gene expression.

Overall, many mechanistic features of dysregulated innate immune responses leading to morbidity and mortality of RSV infections are understood, but its management is still limited to supportive clinical care as there is no effective vaccine or pharmaceuticals for prevention or intervention. Thus, there remains a critical need to further characterize pathways including those generated by oxidative stress to develop effective therapeutic measures to improve outcome of RSV infection. Our study has identified an unprecedented interface among oxidative DNA base damage, initial steps in OGG1-initiated DNA BER, DNA occupancy of transcription factor(s) and RSV-induced IIRs (Fig. 7). Pharmacological inhibition of OGG1 substrate binding, OGG1 silencing and its knockdown significantly decreased IIRs and accelerated recovery of infected experimental animals after RSV infection. Importantly, our findings are substantiated by the effectiveness of the nontoxic OGG1 inhibitor – a small molecule with nanomolar binding affinity to OGG1, which could have clinical utility to decrease RSV-induced exuberant inflammatory responses in humans.

Acknowledgments

Authors acknowledge Professor William Au, editor (University of Texas Medical Branch at Galveston, Galveston, TX, USA), for English editing of the manuscript and scientific advice. We thank Professor Dr. Thomas Helleday (Science for Life Laboratory, Department of Oncology-Pathology, Karolinska Institute, S-171 76, Stockholm, Sweden) for providing the inactive homolog of the OGG1 inhibitor TH5487 for these studies.

Statement of Ethics

Animal experiments were performed according to the NIH Guide for Care and Use of Experimental Animals and approved by the University of Texas Medical Branch (UTMB) Animal Care and Use Committee (Protocol Number: 0807044D).

Conflict of Interest Statement

The authors have no conflicts of interest to declare.

Funding Sources

This work was funded by the NIH National Institute of Allergic and Infectious Diseases NIAID/AI062885 (I.B.; A.R.B.), NIH, Neurological Disorders and Stroke R01 NS073976 (I.B., T.K.H), National Natural Science Foundation of China (Grant No. 32170591 to X.B.), National Natural Science Foundation of China/31900424 (L.P.), National Research, Development and Innovation Office, Hungary (NKFIH K 125337 to A.B.), Royal Physiographic Society of Lund, Sweden, Tore Nilsons Stiftelse 2021-00936, and Lars Hiertas Minne Fund FO2021-0284 (L.T.).

Author Contributions

I. Boldogh, A.R. Brasier. X. Zheng, K. Wang, and W. Hao contributed to conceptualization. I. Boldogh have designed, performed, and analyzed cell culture experiments. X. Zheng, L. Pan, Y. Xue, and W. Hao performed binding assays, immunoprecipitation, ChIPs, and electro mobility shift assays. X. Zheng and K. Wang carried out Flare-qPCR assays. X. Zheng, Y. Xue, K. Wang, and X. Ba cloned, produced, characterized expression vectors, and purified recombinant proteins. L. Pan, K. Wang, and X. Zheng generated OGG1 knockout hSAECs using CRISPR/Cas9 genome editing technology, established, and characterized isolated clones. K. Wang, L. Pan, X. Zheng, T.K. Hazra, and I. Boldogh performed experiments using animals, histology, and cell counts. X. Zheng, Y. Xue, and L. Pan performed qRT-PCR and Bio-Plex assays. Selected experiments using the OGG1 inhibitor, TH5487, were performed by L. Tanner. Statistical analysis, artwork, and figures were done by Y. Xue, X. Zheng, S.A. Vlahopoulos, and A. Bacsi and edited by L. Tanner. Manuscript was written by X. Zheng, K. Wang, I. Boldogh, and Z. Radak and edited by A.R. Brasier, S.A. Vlahopoulos, and L. Tanner. The authors discussed the results and approved the content of the manuscript.

Data Availability Statement

Data on expression of cytokines and chemokines are deposited at the National Center for Biotechnology Information, Gene Expression Omnibus (GEO) number: GSE157630. Upon request, all data sets on which the conclusion of the paper rely are available from the corresponding author.

References

1 Nair H, Nokes DJ, Gessner BD, Dherani M, Madhi SA, Singleton RJ, et al. Global burden of acute lower respiratory infections due to respiratory syncytial virus in young children: a systematic review and meta-analysis. Lancet. 2010;375(9725):1545–55.
2 Tabor DE, Fernandes F, Langedijk AC, Wilkins D, Lebbink RJ, Tovchigrechko A, et al. Global molecular epidemiology of respiratory syncytial virus from the 2017–2018 INFORM-RSV study. J Clin Microbiol. 2020;59(1):e01828–20.
3 Garofalo RP, Kolli D, Casola A. Respiratory syncytial virus infection: mechanisms of redox control and novel therapeutic opportunities. Antioxid Redox Signal. 2013;18(2):186–217.
4 Shi T, McAllister DA, O'Brien KL, Simoes EAF, Madhi SA, Gessner BD, et al. Global, regional, and national disease burden estimates of acute lower respiratory infections due to respiratory syncytial virus in young children in 2015: a systematic review and modelling study. Lancet. 2017;390(10098):946–58.
5 Rosenberg HF, Domachowske JB. Inflammatory responses to respiratory syncytial virus (RSV) infection and the development of immunomodulatory pharmacotherapeutics. Curr Med Chem. 2012;19(10):1424–31.
6 Tian B, Yang J, Zhao Y, Ivanciuc T, Sun H, Garofalo RP, et al. BRD4 couples NF-kappaB/RelA with airway inflammation and the IRF-RIG-I amplification loop in respiratory syncytial virus infection. J Virol. 2017;91(6):e00007–17.
7 Tian B, Yang J, Zhao Y, Ivanciuc T, Sun H, Wakamiya M, et al. Central role of the NF-kappaB pathway in the Scgb1a1-expressing epithelium in mediating respiratory syncytial virus-induced airway inflammation. J Virol. 2018;92(11):e00441–18.
8 Bohmwald K, Espinoza JA, Becerra D, Rivera K, Lay MK, Bueno SM, et al. Inflammatory damage on respiratory and nervous systems due to hRSV infection. Curr Opin Immunol. 2015;36:14–21.
9 Schmidt ME, Varga SM. Modulation of the host immune response by respiratory syncytial virus proteins. J Microbiol. 2017;55(3):161–71.
10 Castro SM, Guerrero-Plata A, Suarez-Real G, Adegboyega PA, Colasurdo GN, Khan AM, et al. Antioxidant treatment ameliorates respiratory syncytial virus-induced disease and lung inflammation. Am J Respir Crit Care Med. 2006;174(12):1361–9.
11 Ivanciuc T, Sbrana E, Casola A, Garofalo RP. Protective role of nuclear factor erythroid 2-related factor 2 against respiratory syncytial virus and human metapneumovirus infections. Front Immunol. 2018;9:854.
12 Ansar M, Ivanciuc T, Garofalo RP, Casola A. Increased lung catalase activity confers protection against experimental RSV infection. Sci Rep. 2020;10(1):3653.
13 Mitra S, Izumi T, Boldogh I, Bhakat KK, Hill JW, Hazra TK. Choreography of oxidative damage repair in mammalian genomes. Free Radic Biol Med. 2002;33(1):15–28.
14 Dizdaroglu M, Coskun E, Jaruga P. Repair of oxidatively induced DNA damage by DNA glycosylases: mechanisms of action, substrate specificities and excision kinetics. Mutat Res. 2017;771:99–127.
15 Steenken S. Structure, acid/base properties and transformation reactions of purine radicals. Free Radic Res Commun. 1989;6(2–3):117–20.
16 Hazra TK, Das A, Das S, Choudhury S, Kow YW, Roy R. Oxidative DNA damage repair in mammalian cells: a new perspective. DNA Repair. 2007;6(4):470–80.
17 McCullough AK, Dodson ML, Lloyd RS. Initiation of base excision repair: glycosylase mechanisms and structures. Annu Rev Biochem. 1999;68:255–85.
18 Izumi T, Hazra TK, Boldogh I, Tomkinson AE, Park MS, Ikeda S, et al. Requirement for human AP endonuclease 1 for repair of 3′-blocking damage at DNA single-strand breaks induced by reactive oxygen species. Carcinogenesis. 2000;21(7):1329–34.
19 Rudd SG, Valerie NCK, Helleday T. Pathways controlling dNTP pools to maintain genome stability. DNA Repair. 2016;44:193–204.
20 Visnes T, Cazares-Korner A, Hao W, Wallner O, Masuyer G, Loseva O, et al. Small-molecule inhibitor of OGG1 suppresses proinflammatory gene expression and inflammation. Science. 2018;362(6416):834–9.
21 Patel JA, Kunimoto M, Sim TC, Garofalo R, Eliott T, Baron S, et al. Interleukin-1 alpha mediates the enhanced expression of intercellular adhesion molecule-1 in pulmonary epithelial cells infected with respiratory syncytial virus. Am J Respir Cell Mol Biol. 1995;13(5):602–9.
22 Livak KJ, Schmittgen TD. Analysis of relative gene expression data using real-time quantitative PCR and the 2(-Delta Delta C(T)) method. Methods. 2001;25(4):402–8.

23 Hao W, Wang J, Zhang Y, Wang C, Xia L, Zhang W, et al. Enzymatically inactive OGG1 binds to DNA and steers base excision repair toward gene transcription. FASEB J. 2020; 34(6):7427–41.
24 Aguilera-Aguirre L, Bacsi A, Saavedra-Molina A, Kurosky A, Sur S, Boldogh I. Mitochondrial dysfunction increases allergic airway inflammation. J Immunol. 2009;183(8):5379–87.
25 Aguilera-Aguirre L, Hao W, Pan L, Li X, Saavedra-Molina A, Bacsi A, et al. Pollen-induced oxidative DNA damage response regulates miRNAs controlling allergic inflammation. Am J Physiol Lung Cell Mol Physiol. 2017;313(6):L1058–L68.
26 Hajas G, Bacsi A, Aguilerra-Aguirre L, German P, Radak Z, Sur S, et al. Biochemical identification of a hydroperoxide derivative of the free 8-oxo-7,8-dihydroguanine base. Free Radic Biol Med. 2012;52(4):749–56.
27 Jamaluddin M, Wang S, Boldogh I, Tian B, Brasier AR. TNF-alpha-induced NF-kappaB/RelA Ser(276) phosphorylation and enhanceosome formation is mediated by an ROS-dependent PKAc pathway. Cell Signal. 2007; 19(7):1419–33.
28 Hao W, Qi T, Pan L, Wang R, Zhu B, Aguilera-Aguirre L, et al. Effects of the stimuli-dependent enrichment of 8-oxoguanine DNA glycosylase1 on chromatinized DNA. Redox Biol. 2018;18:43–53.
29 Pan L, Zhu B, Hao W, Zeng X, Vlahopoulos SA, Hazra TK, et al. Oxidized guanine base lesions function in 8-oxoguanine DNA glycosylase-1-mediated epigenetic regulation of nuclear factor kappaB-driven gene expression. J Biol Chem. 2016;291(49):25553–66.
30 Nowak DE, Tian B, Jamaluddin M, Boldogh I, Vergara LA, Choudhary S, et al. RelA Ser276 phosphorylation is required for activation of a subset of NF-kappaB-dependent genes by recruiting cyclin-dependent kinase 9/cyclin T1 complexes. Mol Cell Biol. 2008;28(11): 3623–38.
31 Amente S, Di Palo G, Scala G, Castrignano T, Gorini F, Cocozza S, et al. Genome-wide mapping of 8-oxo-7,8-dihydro-2′-deoxyguanosine reveals accumulation of oxidatively-generated damage at DNA replication origins within transcribed long genes of mammalian cells. Nucleic Acids Res. 2019;47(1):221–36.
32 Pan L, Hao W, Zheng X, Zeng X, Ahmed Abbasi A, Boldogh I, et al. OGG1-DNA interactions facilitate NF-kappaB binding to DNA targets. Sci Rep. 2017;7:43297.
33 Bacsi A, Aguilera-Aguirre L, Szczesny B, Radak Z, Hazra TK, Sur S, et al. Down-regulation of 8-oxoguanine DNA glycosylase 1 expression in the airway epithelium ameliorates allergic lung inflammation. DNA Repair. 2013;12(1):18–26.
34 Ba X, Bacsi A, Luo J, Aguilera-Aguirre L, Zeng X, Radak Z, et al. 8-oxoguanine DNA glycosylase-1 augments proinflammatory gene expression by facilitating the recruitment of site-specific transcription factors. J Immunol. 2014;192(5):2384–94.
35 Nelson KJ, Klomsiri C, Codreanu SG, Soito L, Liebler DC, Rogers LC, et al. Use of dimedone-based chemical probes for sulfenic acid detection methods to visualize and identify labeled proteins. Methods Enzymol. 2010;473: 95–115.
36 Sebina I, Phipps S. The contribution of neutrophils to the pathogenesis of RSV bronchiolitis. Viruses. 2020;12(8):808.
37 McNamara PS, Flanagan BF, Hart CA, Smyth RL. Production of chemokines in the lungs of infants with severe respiratory syncytial virus bronchiolitis. J Infect Dis. 2005;191(8):1225–32.
38 McNamara PS, Ritson P, Selby A, Hart CA, Smyth RL. Bronchoalveolar lavage cellularity in infants with severe respiratory syncytial virus bronchiolitis. Arch Dis Child. 2003; 88(10):922–6.
39 Zhao Y, Jamaluddin M, Zhang Y, Sun H, Ivanciuc T, Garofalo RP, et al. Systematic analysis of cell-type differences in the epithelial secretome reveals insights into the pathogenesis of respiratory syncytial virus-induced lower respiratory tract infections. J Immunol. 2017; 198(8):3345–64.
40 Jaruga P, Birincioglu M, Rosenquist TA, Dizdaroglu M. Mouse NEIL1 protein is specific for excision of 2,6-diamino-4-hydroxy-5-formamidopyrimidine and 4,6-diamino-5-formamidopyrimidine from oxidatively damaged DNA. Biochemistry. 2004; 43(50): 15909–14.
41 Donley N, Jaruga P, Coskun E, Dizdaroglu M, McCullough AK, Lloyd RS. Small molecule inhibitors of 8-oxoguanine DNA glycosylase-1 (OGG1). ACS Chem Biol. 2015;10(10): 2334–43.
42 Banerjee A, Yang W, Karplus M, Verdine GL. Structure of a repair enzyme interrogating undamaged DNA elucidates recognition of damaged DNA. Nature. 2005;434(7033):612–8.
43 Bespalov IA, Bond JP, Purmal AA, Wallace SS, Melamede RJ. Fabs specific for 8-oxoguanine: control of DNA binding. J Mol Biol. 1999;293(5):1085–95.
44 Kuznetsova AA, Kuznetsov NA, Ishchenko AA, Saparbaev MK, Fedorova OS. Step-by-step mechanism of DNA damage recognition by human 8-oxoguanine DNA glycosylase. Biochim Biophys Acta. 2014;1840(1):387–95.
45 van der Kemp PA, Charbonnier JB, Audebert M, Boiteux S. Catalytic and DNA-binding properties of the human Ogg1 DNA N-glycosylase/AP lyase: biochemical exploration of H270, Q315 and F319, three amino acids of the 8-oxoguanine-binding pocket. Nucleic Acids Res. 2004;32(2):570–8.
46 Wang K, Maayah M, Sweasy JB, Alnajjar KS. The role of cysteines in the structure and function of OGG1. J Biol Chem. 2021 Jan–Jun;296:100093.
47 Bravard A, Vacher M, Gouget B, Coutant A, de Boisferon FH, Marsin S, et al. Redox regulation of human OGG1 activity in response to cellular oxidative stress. Mol Cell Biol. 2006; 26(20):7430–6.
48 Haeberle HA, Takizawa R, Casola A, Brasier AR, Dieterich HJ, Van Rooijen N, et al. Respiratory syncytial virus-induced activation of nuclear factor-kappaB in the lung involves alveolar macrophages and toll-like receptor 4-dependent pathways. J Infect Dis. 2002; 186(9):1199–206.
49 Bitko V, Barik S. Persistent activation of RelA by respiratory syncytial virus involves protein kinase C, underphosphorylated IkappaBbeta, and sequestration of protein phosphatase 2A by the viral phosphoprotein. J Virol. 1998; 72(7):5610–8.
50 Fiedler MA, Wernke-Dollries K. Incomplete regulation of NF-kappaB by IkappaBalpha during respiratory syncytial virus infection in A549 cells. J Virol. 1999;73(5):4502–7.
51 Jozwik A, Habibi MS, Paras A, Zhu J, Guvenel A, Dhariwal J, et al. RSV-specific airway resident memory CD8+ T cells and differential disease severity after experimental human infection. Nat Commun. 2015;6:10224.
52 Olszewska-Pazdrak B, Casola A, Saito T, Alam R, Crowe SE, Mei F, et al. Cell-specific expression of RANTES, MCP-1, and MIP-1alpha by lower airway epithelial cells and eosinophils infected with respiratory syncytial virus. J Virol. 1998;72(6):4756–64.
53 Haeberle HA, Kuziel WA, Dieterich HJ, Casola A, Gatalica Z, Garofalo RP. Inducible expression of inflammatory chemokines in respiratory syncytial virus-infected mice: role of MIP-1alpha in lung pathology. J Virol. 2001; 75(2):878–90.
54 Liu P, Jamaluddin M, Li K, Garofalo RP, Casola A, Brasier AR. Retinoic acid-inducible gene I mediates early antiviral response and Toll-like receptor 3 expression in respiratory syncytial virus-infected airway epithelial cells. J Virol. 2007;81(3):1401–11.
55 Bertolusso R, Tian B, Zhao Y, Vergara L, Sabree A, Iwanaszko M, et al. Dynamic cross talk model of the epithelial innate immune response to double-stranded RNA stimulation: coordinated dynamics emerging from cell-level noise. PLoS One. 2014;9(4):e93396.
56 Tian B, Zhang Y, Luxon BA, Garofalo RP, Casola A, Sinha M, et al. Identification of NF-kappaB-dependent gene networks in respiratory syncytial virus-infected cells. J Virol. 2002;76(13):6800–14.

57 Rallabhandi P, Phillips RL, Boukhvalova MS, Pletneva LM, Shirey KA, Gioannini TL, et al. Respiratory syncytial virus fusion protein-induced toll-like receptor 4 (TLR4) signaling is inhibited by the TLR4 antagonists Rhodobacter sphaeroides lipopolysaccharide and eritoran (E5564) and requires direct interaction with MD-2. mBio. 2012;3(4):e00218–12.
58 Zhang W, Choi Y, Haynes LM, Harcourt JL, Anderson LJ, Jones LP, et al. Vaccination to induce antibodies blocking the CX3C-CX3CR1 interaction of respiratory syncytial virus G protein reduces pulmonary inflammation and virus replication in mice. J Virol. 2010;84(2):1148–57.
59 Sun Y, Jain D, Koziol-White CJ, Genoyer E, Gilbert M, Tapia K, et al. Immunostimulatory defective viral genomes from respiratory syncytial virus promote a strong innate antiviral response during infection in mice and humans. PLoS Pathog. 2015;11(9):e1005122.
60 Komaravelli N, Ansar M, Garofalo RP, Casola A. Respiratory syncytial virus induces NRF2 degradation through a promyelocytic leukemia protein – ring finger protein 4 dependent pathway. Free Radic Biol Med. 2017;113:494–504.
61 Hosakote YM, Liu T, Castro SM, Garofalo RP, Casola A. Respiratory syncytial virus induces oxidative stress by modulating antioxidant enzymes. Am J Respir Cell Mol Biol. 2009;41(3):348–57.
62 Hall DB, Holmlin RE, Barton JK. Oxidative DNA damage through long-range electron transfer. Nature. 1996;382(6593):731–5.
63 Ba X, Boldogh I. 8-oxoguanine DNA glycosylase 1: beyond repair of the oxidatively modified base lesions. Redox Biol. 2018;14:669–78.
64 Fleming AM, Burrows CJ. 8-Oxo-7,8-dihydroguanine, friend and foe: epigenetic-like regulator versus initiator of mutagenesis. DNA Repair. 2017;56:75–83.
65 Roychoudhury S, Pramanik S, Harris HL, Tarpley M, Sarkar A, Spagnol G, et al. Endogenous oxidized DNA bases and APE1 regulate the formation of G-quadruplex structures in the genome. Proc Natl Acad Sci U S A. 2020;117(21):11409–20.
66 Sun Y, López CB. The innate immune response to RSV: advances in our understanding of critical viral and host factors. Vaccine. 2017;35(3):481–8.
67 Amouroux R, Campalans A, Epe B, Radicella JP. Oxidative stress triggers the preferential assembly of base excision repair complexes on open chromatin regions. Nucleic Acids Res. 2010;38(9):2878–90.
68 Brasier AR, Boldogh I. Targeting inducible epigenetic reprogramming pathways in chronic airway remodeling. Drugs Context. 2019;8.
69 Choudhary S, Boldogh S, Garofalo R, Jamaluddin M, Brasier AR. Respiratory syncytial virus influences NF-kappaB-dependent gene expression through a novel pathway involving MAP3K14/NIK expression and nuclear complex formation with NF-kappaB2. J Virol. 2005;79(14):8948–59.
70 Brasier AR. RSV reprograms the CDK9•BRD4 chromatin remodeling complex to couple innate inflammation to airway remodeling. Viruses. 2020;12(4):472.
71 Mann M, Roberts DS, Zhu Y, Li Y, Zhou J, Ge Y, et al. Discovery of RSV-induced BRD4 protein interactions using native immunoprecipitation and parallel accumulation-serial fragmentation (PASEF) mass spectrometry. Viruses. 2021;13(3):454.
72 Bruner SD, Norman DP, Verdine GL. Structural basis for recognition and repair of the endogenous mutagen 8-oxoguanine in DNA. Nature. 2000;403(6772):859–66.
73 Qin S, Lin P, Wu Q, Pu Q, Zhou C, Wang B, et al. Small-molecule inhibitor of 8-oxoguanine DNA glycosylase 1 regulates inflammatory responses during pseudomonas aeruginosa infection. J Immunol. 2020;205(8):2231–42.